Stimulating *In Situ* Groundwater Bioremediation via Sparging: Gas flow, Groundwater flow, and Mass Transfer in the Biosparge Zone

by

Michael F. Hayes, Jr.

Submitted to the Department of Civil and Environmental Engineering
in Partial Fulfillment of the Requirements for the Degree of

Master of Science in Civil and Environmental Engineering

at the

Massachusetts Institute of Technology
February 1996

Signature of Author _____
Michael F. Hayes, Jr.
January 19, 1996

Certified By _____
Lynn Gelhar
Professor, Civil and Environmental Engineering
Thesis Supervisor

Accepted By _____
Joseph M. Sussman
Chairman, Departmental Committee on Graduate Studies

Stimulating *In Situ* Groundwater Bioremediation via Sparging: Gas Flow, Groundwater Flow, and Mass Transfer in the Biosparge Zone

by

Michael F. Hayes, Jr.

Submitted to the Department of Civil and Environmental Engineering on January 19, 1996 in Partial Fulfillment of the Requirements for the Degree of Master of Science in Civil and Environmental Engineering

Abstract

Aquifer sparging consists of pumping a gas or gas mixture, usually air, into a contaminated groundwater aquifer. As the sparge gas rises through the saturated zone, some fraction of the gas dissolves into the groundwater and some fraction of the groundwater contamination evaporates into the gas.

When used primarily to deliver compounds necessary for bioremediation into solution, aquifer sparging is sometimes referred to as "biosparging." The purpose of this study is to investigate the feasibility of stimulating *in situ* bioremediation of large-scale groundwater contamination plumes via biosparging.

Based on the premise that sparging results in stable, discrete gas channels flowing from the point of injection to the water table, a conceptual mass transfer model is developed. The model is used to investigate the feasibility of stimulating bioremediation in a large trichloroethylene (TCE) plume on Cape Cod, Massachusetts.

The major conclusion of this work is that biosparging may offer a viable method for stimulating bioremediation in large-scale groundwater plumes. The factor most crucial to the success of the technology is the spatial distribution and size of the sparge gas channels.

Additional effects of the channel flow regime are investigated. Expressions relating channel size and density to air saturation and hydraulic conductivity are developed. Variation in channel size and vertical gas specific discharge is explored. The effects of sparging on groundwater flow direction is investigated using finite element analysis software.

Thesis Supervisor: Lynn Gelhar
Title: Professor

Acknowledgments

Ed Pesce and Mike Minior of the Massachusetts Military Reservation and Ken Till of OpTech have been very helpful in providing information on the Cape Cod site used in the case study. Their assistance is greatly appreciated.

Graduate work at the Parsons Lab is very much a team effort. Students and faculty of every discipline are always willing to offer a new perspective on any aspect of a research problem. Thank you to the fellow students and faculty who helped me along the way.

On a very regular basis during the last year, Dr. Lynn Gelhar took the time to impart upon me his considerable knowledge of hydrology and his knack for critically examining scientific information. Thank you for patiently showing me the ropes.

Were it not for the love of learning and belief in my abilities taught to me by my parents, I would never have arrived at MIT. Thank you for laying the foundation of my education long before I knew how important it would be.

My wife, Anne, supported my original decision to return to graduate school and has continued to support me through both "good times and bad." This experience has reminded me yet again of how fortunate I am in this regard. Thank you for everything.

Table of Contents

List of Figures

List of Tables

Chapter One

Introduction

Groundwater throughout the world is contaminated with a diverse array of xenobiotic compounds. One of the more promising methods available to attenuate this contamination is *in situ* ("in place") bioremediation. This technology capitalizes on the ability of aquatic microorganisms to reduce or eliminate a pollutant's toxicity as they grow and reproduce.

All aquifers investigated thus far support a microbial population, and microorganisms with the ability to degrade many of the groundwater pollutants generated by human activity have been identified [Bedient et al., 1994]. This is true despite the fact that the majority of existing bacterial species have never been isolated, much less studied [National Resources Council, 1993]. Genetic engineering techniques are beginning to enable us to improve the degradation capabilities of bacteria. In short, there is good reason to believe that an inability to identify a suitable microorganism will not be the limiting factor in future applications of bioremediation.

Unfortunately, there is a large disparity between a microorganism transforming a pollutant in a laboratory experiment and the same process occurring on a large scale in an aquifer. In natural environments, even if an appropriate native microorganism population exists, bioremediation is frequently limited by a shortage of the chemical compounds necessary for microbial growth: organic carbon, nutrients, and electron acceptors or donors. When bioremediation is limited by the unavailability of one or more of these crucial compounds, a successfully engineered bioremediation system must deliver the compounds into solution in the groundwater. This work focuses on one type of delivery system, aquifer sparging.

1.1 Aquifer Sparging

First proposed in 1974 [Johnson, 1994] and first used in the mid-1980's [Ahlfield et al., 1994], aquifer sparging consists of pumping a gas or gas mixture, usually air, into a contaminated aquifer. As the gas rises through the saturated zone, two mass transfer processes occur. Some fraction of the gas dissolves into the groundwater, and some fraction of contamination in the groundwater evaporates into the gas.

When used primarily to remove contamination via contaminant evaporation, aquifer sparging is frequently referred to as "air-stripping." The newly-contaminated air travels up through the aquifer to the vadose zone, where an extraction system captures the gaseous contaminants and pumps them to the surface for treatment. This type of system is frequently referred to as In-Situ Air Sparging - Soil Vapor Extraction (IAS-SVE).

IAS-SVE has the potential to reduce the concentration of volatile chemicals in an aquifer fairly quickly. Unfortunately, this process has several drawbacks. First, stripping does not work well with less volatile groundwater contaminants. Second, it requires the additional expense and complexity of an extraction system in addition to the air injection system. Third, the process becomes less efficient as contamination concentrations decrease, and air stripping may not always be able to lower contamination levels below regulatory limits. In cases where non-aqueous phase liquid (NAPL) contamination exists, air-stripping may lower the initial dissolved contaminant concentration, but subsequent NAPL dissolution will continue to provide a source of groundwater contamination over the long term. At sites with NAPL contamination, air stripping may exhibit limitations similar to those seen in pump and treat systems [Boersma et al., 1995]. Fourth, and perhaps most importantly, air stripping does not actually remediate contamination, it simply moves it into another medium that must be subsequently remediated. If time is a critical factor, then the benefits of air stripping may outweigh its drawbacks. When

time is not crucial, the use of sparging to stimulate in situ bioremediation may offer a better alternative.

When used primarily to deliver compounds necessary for bioremediation into solution, aquifer sparging is sometimes referred to as "biosparging." This technology introduces sparge gas into the aquifer at relatively low rates in an attempt to deliver the required compounds while reducing the rate of contaminant volatilization. At lower volatilization rates, the gaseous contaminant flux to the aquifer above the plume may be low enough so that vadose zone biodegradation or physical dispersion will obviate the need for a vapor recovery system. In-situ biodegradation is a highly attractive technology because it can achieve extremely low clean-up levels and because it destroys contaminants in place instead of simply immobilizing them or moving them to another location.

1.2 The Biozone Concept

Limited only by the natural variety in the geology of water-bearing formation, aquifer characteristics vary dramatically. The heterogeneous nature of most aquifers and natural variation in the processes that affect contaminant transport result in irregularly shaped plumes with contaminant concentrations varying both in time and space. Nonetheless, investigations of less complex, hypothetical plumes may yield valuable insights. This work considers a "generic" plume with a characteristic rectangular width, thickness and depth at its leading edge, as shown in Figure 1 (relative vertical scale is exaggerated). The direction of groundwater flow and the primary plume axis are parallel to the x axis.

Sparging systems are frequently implemented within the boundaries of a contaminant plume to minimize remediation time. For relatively small plumes, this may be an appropriate approach. Some plumes, however, encompass tens of thousands of square feet. The maximum radial distance impacted by a sparging well is usually on the order of tens of feet [API, 1995], making a direct approach impractical. When faced with large plumes, emphasis is frequently

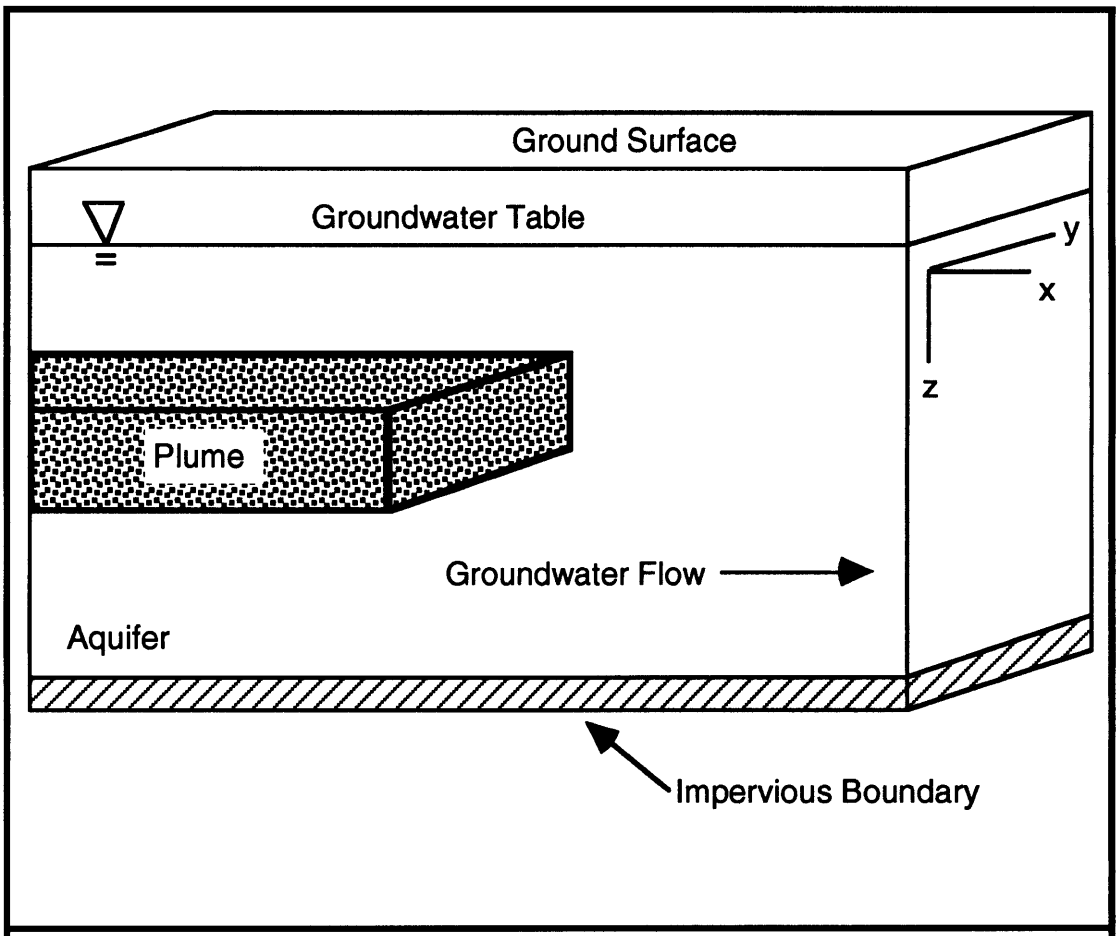

Figure 1 - Hypothetical Groundwater Plume

placed on containing the plume to prevent further contaminant migration. Remediation of the aquifer may be accomplished over a longer period.

Consider again the aquifer shown in Figure 1. To prevent further migration of the plume in the short term, some sort of barrier to contaminant transport must be placed hydraulically downgradient. To remediate the plume over the long term, some sort of treatment must be brought to bear on the contamination that already exists.

Both of these tasks may be accomplished simultaneously. Assume microorganisms capable of remediating the plume exist in the aquifer at low concentrations due to a lack of one or more critical compounds. By biosparging a controlled gas mixture in an area immediately downgradient of and perpendicular to the leading edge of the plume, the microorganism population can be provided with the compounds necessary to degrade the plume as they grow and reproduce. The zone of increased biological activity, or "biozone," acts as a barrier to further contamination migration. Figure 2 illustrates a biozone created by a series of vertical sparge wells or a single horizontal sparge well.

Because the biozone is permeable to groundwater flow, it acts as an in-situ treatment facility, with natural groundwater gradients providing the "pump" to deliver contaminated water for remediation. Thus, the biozone creates a barrier beyond which contamination can not spread and slowly remediates contamination as it is transported into the biozone by groundwater flow.

The previous two paragraphs, which outline the biozone concept, contain several "make or break" assumptions. Each of the following conditions must be met for the biozone to be effective:

1. The time spent by the plume in the biozone must be sufficient to allow bioremediation to reduce contaminant concentrations below regulatory limits.

2. Sparging must transfer a sufficient mass of the necessary biological components into solution to allow for continuous biodegradation of the maximum plume concentration.

3. Sparge gas exiting the top of the biozone must not cause air concentrations above ground to exceed regulatory limits.

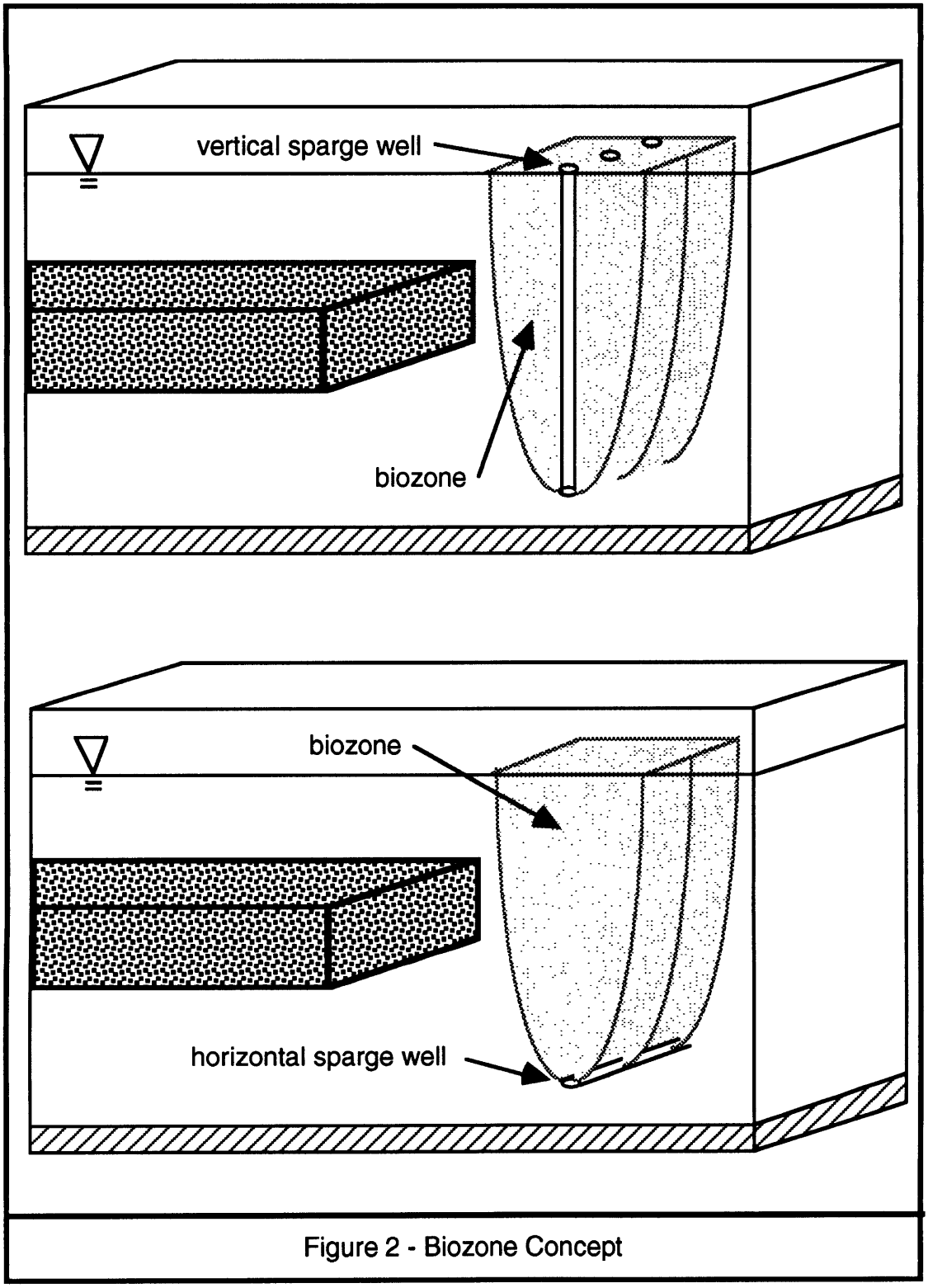

Figure 2 - Biozone Concept

4. Changes in hydraulic conductivity caused by sparging must not cause the plume to flow around or under the biozone.

Each of these conditions will be tested in subsequent chapters. If they hold, the biozone concept may offer a viable solution to large scale groundwater contamination challenges.

1.3 Thesis Organization

The purpose of this study is to investigate the feasibility of stimulating in situ bioremediation of a contaminated aquifer through the introduction, via biosparging, of compounds necessary for microbial activity. In Chapters 2 and 3 the basic concepts of bioremediation and two-phase flow in porous media are developed to provide a background for subsequent discussion. The results of laboratory and field investigations of air sparging phenomena are then presented and discussed in Chapter 4. Previously developed models of sparging mass transfer processes are also examined.

The premise that sparging results in stable, discrete, contiguous gas channels is investigated in Chapter 5. A conceptual mass transfer model employing gas channel elements is developed. The model is used to investigate the effects of a variety of design variables on sparging systems.

A case study is evaluated in Chapter 6 to illustrate theoretical concepts developed and to test the practical outcome of that theory. Chapter 7 summarizes conclusions and makes recommendations for future research.

Chapter Two

Bioremediation

Chapter 1 briefly discussed the ability of microorganisms to degrade groundwater pollutants. This chapter provides an introduction to the methods by which these biochemical transformations occur. The biotransformation of one of the most ubiquitous groundwater contaminants, trichloroethylene (TCE), is then discussed.

2.1 Biochemical Transformations

Bacteria can exist under a wide range of environmental conditions, such as temperature, pH, and pressure. To thrive, however, bacteria need a sufficient supply of three things: nutrients, an organic carbon source, and an energy source. Nutrients necessary for bacterial life include nitrogen, phosphorous, calcium, magnesium, iron, and trace elements [Bedient et al., 1994]. Organic carbon may be obtained from any organic molecule, such as CH_4. Bacteria usually obtain their energy by catalyzing reactions that break chemical bonds and transfer the liberated electrons from one compound to another. The bacteria appropriate energy during the electron transfer. Note that from a bacteria's point of view, where electrons come from and where they end up is not as important as the process of electron transfer.

Bacteria generally catalyze reactions through two methods. In the first, bacteria manufacture enzymes that lower the free energy of activation necessary for the reaction to proceed, thereby increasing the reaction rate [Schwarzenbach, et al., 1993]. The enzyme does not change the educts or the products, and it is not consumed in the reaction. The catalyzed reaction simply proceeds much faster than the same uncatalyzed reaction, sometimes

by as much as a factor of 10^9 [Schwarzenbach, et al., 1993]. In the second method, bacteria actually change one or more of the reaction educts into a more reactive form. In this case, biologic activity actually results in a slightly different as well as faster reaction than the original.

The compound acting as an energy source and electron donor is oxidized, while the compound accepting the electrons is reduced. When a compound provides both organic carbon and energy to bacteria, it is referred to as a primary substrate. Petroleum hydrocarbons, for instance, serve as primary substrates for a variety of bacteria found in groundwater. If a contaminant may be utilized as primary substrate, stimulating bioremediation requires only the supply of an appropriate electron acceptor and any necessary nutrients. One of the most common electron acceptors is oxygen.

Many common groundwater contaminants do not make good primary substrates. Fortunately, the enzymes produced by bacteria to catalyze one reaction sometimes fortuitously catalyze contaminant transformations as well. In this case, the contaminant is referred to as a secondary substrate, and the primary/secondary substrate system is referred to as cometabolism. If a contaminant is degraded as a secondary substrate, stimulating bioremediation requires the supply of an appropriate primary substrate, an appropriate electron acceptor, and any necessary nutrients.

There is an important side benefit when contaminants are secondary rather than primary substrates. The rate of disappearance of a primary substrate will eventually decrease as it is utilized, since the microorganism population will decline when the primary substrate concentration reaches a low enough level. The transformation of secondary substrates can be stimulated regardless of how low their concentration falls; as long as primary substrate is provided, biotransformation can be maintained.

In some cases, a contaminant may serve as the electron acceptor and be transformed through a reduction reaction. In this case, stimulating

bioremediation requires the supply of an appropriate electron donor and any necessary nutrients.

2.2 TCE Cometabolism

Chlorinated solvents, such as TCE, have been used throughout the world for decades in a variety of industrial processes. This widespread use has resulted in uncontrolled releases to the environment, and chlorinated solvents are common groundwater contaminants. In fact, according to at least one estimate, TCE is the most common organic groundwater contaminant in the United States [Wackett, 1995].

Due to its prevalence, possible biodegradation mechanisms for TCE have been studied extensively. One of the most prevalent transformers of TCE are bacteria known as methanotrophs. These bacteria utilize methane as their primary substrate, obtaining energy as they break it down through a series of steps to carbon dioxide and water [Henry and Grbic-Galic, 1994]. The first step in this process, the transformation of methane to methanol, is catalyzed by the enzyme methane monooxygenase (MMO).

Bioremediation of TCE by methanotrophs is possible because unlike many enzymes, MMO attacks a wide variety of compounds. Numerous studies [e.g. Wackett, 1995; Henry and Grbic-Galic, 1994] have concluded that MMO adds a single molecule of oxygen to TCE to form the relatively unstable TCE epoxide molecule, which quickly decomposes into nontoxic compounds. The requirement for the stimulation of TCE cometabolism is therefore a supply of methane, oxygen, and any necessary nutrients.

Chapter Three

Two-phase Phenomena in Porous Media

Many hydrology texts [e. g. Bear, 1972; Dullien, 1979; Greenkorn, 1983] include a separate section on multiphase flow of immiscible fluids in porous media. This chapter will not attempt to compete with reference texts; rather, the goal here is to review and explore some of the basic ideas that are necessary for development of two-phase mass transfer concepts in Chapter 5.

Prior to the introduction of a sparge gas below the water table, the pore spaces between grains of aquifer material are considered to be full of water. When gas enters the aquifer, it must necessarily displace some of the water from the pore spaces, and an interface between the two fluids is formed.

Molecules at the interface will be attracted to each other and to the substance on "the other side" of the interface. The work necessary to separate one substance from another (per unit area interface) is referred to as the surface tension.

Experiments have shown that when a fluid invades pores already filled with another fluid, one fluid or the other will preferentially cover, or "wet" the grain surface. In the gas/water system created by sparging, water is the wetting fluid and the gas is the non-wetting fluid. No matter how much gas is pumped through the pores, some small amount of water will coat the grains and accumulate slightly in the grain contact points.

Dullien [1979] uses Laplace's equation to show that because of the existence of surface tension an interface with a characteristic mean radius of curvature will form to maintain mechanical equilibrium between two fluids. The fluids

will be at different pressures on either side of the interface, and the fluid on the concave side will have a pressure which is greater than the pressure on the convex side. In natural systems, the water is on the convex side of the gas/water interface and the pressure in the water is slightly lower than the gas. The difference between these two pressures is called the capillary pressure:

$$p_c = p_g - p_w$$

where

p_c = capillary pressure

p_g = pressure in the sparge gas

p_w = pressure in the groundwater

Bear [1972] refers to the capillary pressure as a "measure of the porous medium to suck in the wetting fluid phase or to repel the nonwetting phase." Greenkorn [1983] derives expressions for the capillary pressure in three interface geometries (planar, cylindrical, and spherical) representing various pore shapes. In all cases, the capillary pressure is directly proportional to the surface tension and inversely proportional to a characteristic radius of the curved interface surface. As discussed earlier, the surface tension is a function of the two fluids. The characteristic interfacial radius is therefore a function of the fluids present, the amount of each fluid present, and the pore size.

As pore size decreases, the characteristic radius of the interface must also shrink, resulting in an increasing capillary pressure. A reduction in water content in the pores (due to sparging, for instance) will result in the water moving further back into the space where grains contact, further reducing the characteristic radius and increasing capillary pressure. Laboratory experiments provide information on this second effect.

The saturation ratio of a fluid α (S_α) is defined as the fraction of the total pore space filled with the fluid. Curves describing the relationship between capillary pressure and saturation ratios are determined experimentally. A

curve representing the change in capillary pressure as gas enters an initially saturated porous media is shown in Figure 3.

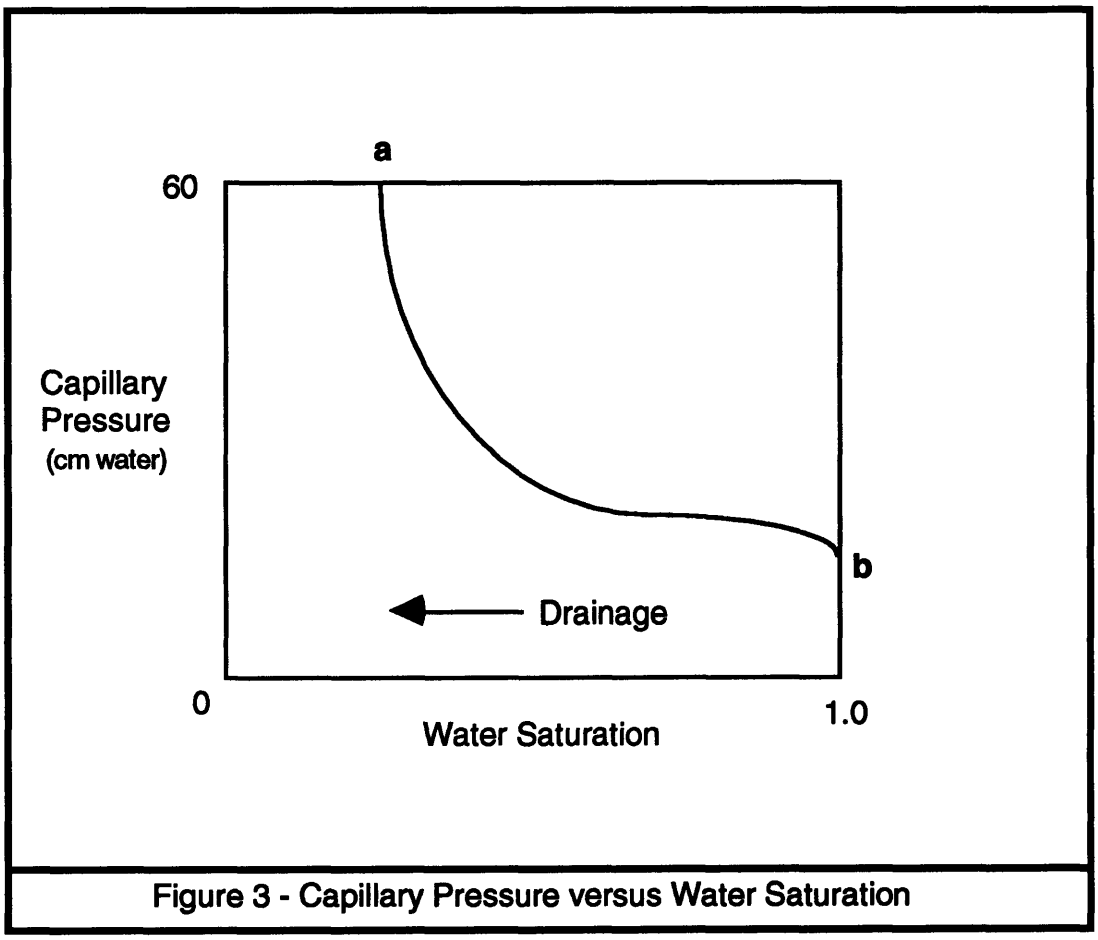

Figure 3 - Capillary Pressure versus Water Saturation

As the water saturation is reduced, capillary pressure increases as predicted above. There are several aspects of the curve in Figure 3 that deserve further discussion.

The asymptotic behavior of the curve at point **a** indicates the minimum, or irreducible, wetting fluid saturation. Regardless of further rise in capillary pressure, surface tension effects will "hold" some of the non-wetting fluid in the pore spaces. Point **b** indicates that a certain capillary pressure must be reached before any nonwetting fluid movement into the pore space may occur. This is consistent with Bear's [1972] characterization of capillary pressure as a

measure of the medium's tendency to repel the nonwetting fluid. This critical capillary pressure is referred to in the literature as the entry, bubbling, displacement, or threshold pressure. This work will use the term entry pressure and the symbol p_e.

So far the effects of wetting and nonwetting fluid flow have been ignored. To visualize such flow, consider a situation where one-half of the void volume is filled with water and the other one-half with air. Because the two fluids are competing for pore space, neither will be find the material as permeable as if they were the only fluid flowing. The ratio between how permeable a porous media appears to a fluid at 100 percent saturation relative to its permeability at a reduced saturation is known as the relative permeability. To describe the flow of a fluid α in unsaturated porous media, Darcy's law must be modified with a relative permeability term to account for the affect of this "flow competition."

$$\vec{q}_\alpha = -\frac{k_\alpha k}{\mu_\alpha}(\nabla p_\alpha - \rho_\alpha \vec{g})$$

where

$\vec{q}_\alpha$ = specific discharge vector of fluid α $\left(\frac{L}{T}\right)$

k_α = relative permeability of fluid α

k = intrinsic permeability of the porous media $\left(L^2\right)$

p_α = fluid α pressure $\left(\frac{M}{L\text{-}T^2}\right)$

μ_α = fluid α dynamic viscosity $\left(\frac{M}{L\text{-}T}\right)$

ρ_α = fluid α density $\left(\frac{M}{L^3}\right)$

$\vec{g}$ = gravity acceleration vector $\left(\frac{L}{T^2}\right)$

This Darcy equation and its three dimensional extensions may be combined with conservation of mass expressions to derive equations for mass transport in both phases through unsaturated porous media. These equations, which have been studied extensively, are usually applied to unsaturated conditions such as those that exist in the vadose zone, where water and air saturation values are averaged over many pore volumes. The coupled, nonlinear nature of the equations governing two-phase flow generally requires the of numerical solution methods (see, for example, Binning et al. [1995], Sleep and Sykes [1989]), although some exact solutions have been derived (e.g. McWhorter and Sunada [1990]). As discussed in Chapter 4, it is not yet clear if classical two-phase flow equations are applicable to the portion of the aquifer impacted by the flow of sparge gases.

Chapter Four

Air Sparging: State of the Art

Despite several years of study, the physics of injected sparge gas in the underground environment is not well understood. This chapter begins with a discussion of previous field and laboratory investigations into sparging flow phenomena. Current conceptual models of sparging mass transfer are then presented and discussed.

4.1 Laboratory Investigations

Very few investigations of sparging phenomena have been conducted in research labs. A sparging experiment faces the challenges of any "sandbox" study, such as the extreme difficulty and significant cost of attempting to create easily monitored, natural heterogeneous aquifer conditions at reasonable scales. Sparging studies also face the additional hurdle of sensing the movement of injected gas through the experimental porous media. In fact, no results of three-dimensional sensing of discrete air flow paths have been reported.

Several studies have compromised by reducing the scope of the investigation to two dimensions. Ji et al [1993] used such an approach in what is one of the most-referenced studies in the sparging literature. Water-wet glass beads with specified diameters were packed between two panes of Plexiglas measuring 34.5 inches (in) tall by 28.75 in wide. The Plexiglas panes were held 1 in apart by a series of spacers and air was injected into the center of the bottom of the enclosed space through a 1 in long by 0.5 in diameter diffuser. The apparatus was back-lit and air flow upward through the glass beads was observed visually.

Three experiments on beds of uniform glass beads were run to investigate the effect of grain size on air flow. Air moving through 4 millimeter (mm) diameter glass beads flowed in a bubbling motion, 0.75 mm beads resulted in steady, distinct, air flow channels, and an intermediate bead size of 0.2 mm resulted in a mixed flow regime exhibiting both discrete air channels above the sparge point and bubbling flow at greater radial distances. In all cases, the flow was roughly symmetrical around a centerline above the diffuser. From these results, the authors concluded that a grain size of approximately 2 mm delineated the transition from bubbling to channel flow. A grain size of 2 mm is frequently used to distinguish between gravel and sand in soil classification schemes [Ji et al., 1993].

Pressure in all cases was increased gradually so entry pressures could be measured. The 4 mm beads exhibited no measurable entry pressure, the 0.75 mm beads exhibited an entry pressure of 6 in of water, and no entry pressure was recorded for the 2 mm beads. For channel flow, increased air injection rates resulted in new channel formation and lateral spreading of the channel pattern. At high flow rates with 0.75 mm beads, the authors estimated that air and water saturations were approximately equal at 0.5.

A second series of experiments utilized mixtures of glass beads with several diameters. A variety of methods were employed to maximize the random distribution of beads and therefore pore diameters. An asymmetric channel flow pattern developed, with channel widths on the order of 10 to 20 pore diameters. Higher air flow rates caused some increase in the lateral spreading of channels and the channel density but no increase in channel size.

A third series of experiments was run to investigate the effect of horizontal, low-permeability lenses. The lenses were created by arranging thin layers of 0.4 mm and 0.2 mm beads in a bed of 0.75 mm beads. As air flowed up in channels and encountered a lens, air accumulated under the lens and began to move laterally until the edge of the lens was reached. At this point the air

again began to travel upward in stable channels. Areas directly above low permeability lenses were not directly impacted by airflow.

Additional lab studies support the theory that discrete channels form. Plummer [1994] studied air sparging using an apparatus similar to that of Ji et al. [1993]. Plummer [1994] also observed discrete, relatively stable channels forming in saturated beds of both glass beads and beach sand. Increasing flow rates in this study did not result in significantly greater lateral channel spreading; rather, the density of channels increased. When sparging was discontinued and then reinitiated after a resting period of several hours, the channel distribution did not change significantly.

An interesting phenomenon noted by Plummer [1994] was the presence of "dead-end" channels, which traveled a large percentage of the distance to the water table and then simply stopped. Sketches of the Ji et al. [1993] study results also indicate such dead-end channels, although they are not mentioned by the authors. If they are numerous, these stagnant channels could have significant impact on mass transfer between the gas and water phases.

Although these studies provide valuable insight into the movement of air through porous media, sources of inaccuracy do exist. Plummer [1994] noted that even if a bed of glass beads has a porosity, intrinsic permeability, hydraulic conductivity, and bulk density similar to a natural porous medium, the smaller particle-to-particle friction of glass beads results in relatively easy bead movement during sparging. This makes physical sense. A two-foot deep saturated bed of glass beads under the equivalent of 9 in of soil overburden (the amount used by Plummer [1994] - Ji et al. [1993] used even less) resembles a large quantity of water-lubricated ball bearings as much as it resembles a 50-foot deep geological deposit that has consolidated over several million years. Air flow rates through glass beads in the Plummer [1994] study were 2.5 to 3 times higher than through sand for similar injection pressures; he attributed this to the beads' lower resistance to flow.

At low air flow rates, however, the inaccuracy caused by the use of underburdened glass beads is reduced, and some insight is definitely gained from experiments like those described above. It is simply difficult to judge how accurately these experiments mimic the three-dimensional movement of sparge gases in heterogeneous aquifers.

4.2 Field Investigations

Description of numerous sparging operations are available in the public domain. The majority are concerned with developing a better understanding of the extent of radial air movement away from a vertical sparge well and related hydrological effects. A large number investigate the efficacy of one or both of the remediation processes described in Chapter 1 (air stripping and stimulation of bioremediation). Representative examples of these investigations are presented below. A quick overview of recent work in the sparging field may be obtained by reading Hinchee [1994a] and Hinchee et al. [1995].

4.2.1 Visual Measurement of Sparging Zone of Influence

Imaging hypothetical sparge gas channels with diameters of several millimeters in field scale settings clearly presents a difficult technical challenge. Leeson et al. [1995] conducted a simple but effective experiment to examine the zone of influence of a vertical sparge well as a function of depth and flowrate.

A 1.25 in inner diameter stainless steel well point with a 1.5 foot screen was driven to depths of 6, 10, and 17.5 feet in tidal flat with shallow standing water. The soil was described as relatively uniform sand. Air was injected at flowrates of 2.5, 6, 10, 20, 24, and 31 cubic feet per minute (cfm) and the location and rate of appearance of bubbles in the standing water at the site were recorded visually.

At all depths and at all flowrates, a central area of high bubbling was observed within one or two feet of the injection well. Lower rates of bubbling occurred sporadically outside of this area in a generally symmetrical pattern. The authors conclude that increased injection depth resulted in an increased zone of influence, while an increased flowrate caused more channels to form without a significant increase in the zone of influence. Bubbles traveled a maximum radial distance of approximately 16 feet when air was injected at a depth of 17.5 feet at a flowrate of 31 cfm. In all cases, the location of bubbles and their frequency of occurrence did not vary much with time. Interrupting continuous airflow with several short pulses caused the number of bubble sites to increase without significantly changing the zone of influence.

This study seems to present three-dimensional results analogous to the two-dimensional mixed flow regime encountered by Ji et al. [1993]. The practically continuous flow near the sparge point may be the result of a dense central network of air channels, while the slower bubbling at larger radii may be the result of bubbling flow. Alternatively, the slower bubbling may be the manifestation of extremely low but continuous flow resulting in slow-forming bubbles that must reach a certain size to detach from the soil surface and flow to the surface of the standing water. Thus, this field study may lend some credence to the gas channel flow theory.

4.2.2 Air Sparging in Uniform Sand

At this site in southern Alaska, Acomb et al., [1995] injected air 15 feet below the water table in an unconfined aquifer at various flowrates. Soils at the site consisted of "uniform, fine sand" with a porosity of approximately 40 percent. A series of vertical observation pipes were installed along a single radius emanating from the sparge well at distances of 4, 7, 11, and 15 feet. For a given experimental run, a fast neutron source/thermal neutron detector was lowered into the pipes and soil moisture measurements were obtained at two foot intervals. Moisture in a 3 to 6 in radius around the pipe slows (thermalizes) a certain percentage of the emitted neutrons and reflects them back to the detector; the rate of thermal neutron reflection is proportional to

moisture content. Dissolved oxygen and pressure were also monitored at a series of monitoring wells at various distances from the sparge well. Field data indicated the following:

- Air saturation was not uniform over the affected zone. Air saturation decreased from a high of approximately 40 percent within a few feet of the well to 0 percent approximately 15 feet from the well. This is consistent with the higher central bubbling radius observed by Leeson et al. [1995].

- The radial zone of air saturation expanded to a maximum in approximately one hour and then decayed to a smaller, steady state zone over the next few hours. The magnitude of collapse was on the order of 2-4 feet.

- Increasing air injection flow caused a small increase in the zone of influence, but the predominant effect was to further desaturate the volume closest to the sparge well. This result is consistent with the experimental results of both Plummer [1994] and Lesson et al. [1995]. The steady-state sparge zone radius varied from approximately 11 feet at an injection rate of 4 cfm to 15 feet at 16 cfm.

- An increase in dissolved oxygen from near 0 milligrams per liter (mg/l) to 5 mg/l was detected at flowrates of 8, 12, and 16 cfm within 15 feet of the sparge well. No increase in dissolved oxygen was noted in a monitoring well located 20 feet from the sparge well. This shows a good correlation between increasing dissolved oxygen levels and the boundary of the sparge zone.

- Increases in saturated zone pressure and water table elevation were measured across the study site upon initiation of sparging. The pressure increases reached a peak within approximately 30 minutes, decayed to below presparge levels over the course of several hours, and then stabilized at presparge pressures. Water table mounding was observed over 60 feet from the sparge well, indicating that a change in water table level is not a good indication of the boundary of the sparge zone.

This example was chosen because it illustrates many of the concepts about which a consensus appears to exist in sparging practice. These concepts include:

- Upon the initiation of sparging, a local, transient mounding of the water table occurs. The water table returns to approximately its original level on the order of hours. In many cases, the water table exhibits an underdamped response, falling to below its original level before reaching equilibrium. [Clayton, 1995; Lundegard, 1994; Lundegard 1995]

- Injected gas generally moves radially and vertically away from the injection point, lowering the water saturation in the sparge zone. The air invades the pore spaces in via a network of sparge gas channels [Johnson et al., 1993; Hinchee, 1994b; Ahlfeld, 1994; Lundegard, 1994; API, 1995; Boersma, 1995]

- When sparging is terminated, a transient, local depression of the water table occurs. The water table returns to its initial level within a few hours. [Clayton, 1995; Lundegard, 1994; API 1995]

4.2.3 Large-Scale Biosparging with Horizontal Wells

Hazen [1995] published an summary of this investigation. Over a 13-month period in 1992 and 1993, a large-scale sparging field investigation was conducted at the U. S. Department of Energy Savannah River Site near Aiken, South Carolina. A sewer line used for approximately 30 years leaked chlorinated solvents into the vadose zone. The contamination migrated downward, eventually forming a groundwater plume encompassing over one square mile.

One 300-foot long horizontal injection well was installed at a depth of 175 feet below ground surface (bgs) and one 175-foot long extraction well was installed at a depth of 80 feet bgs. Both wells were screened over most of their lengths. Air was injected at approximately 200 cfm and extracted at 240 cfm.

During different phases of the investigation, the injected air was amended with low percentages (1 or 4 percent) of methane and, in some cases, gaseous nutrients (nitrous oxide and triethyl phosphate). The system was fully automated and required only about 7 hours of operator time per week for analytical performance monitoring. Electrical resistance tomography measurements of air saturation indicated that the sparge gas flow paths extended laterally to as far as 100 feet from the injection well, while methane was detected at distances over 500 feet from the injection well [U. S. DOE, 1995].

Eddy et al., [1991] describe the geology and hydrogeology at the site. The coastal plain sediments at the site consist of laterally discontinuous sands, sandy clays, clayey sands, and clays. The water table at the test site is encountered at approximately 130 feet bgs and the shallow water bearing units are classified into unconfined, semi-confined, and confined zones.

The Savannah River investigation demonstrates the feasibility of using horizontal wells to stimulate in situ bioremediation at depths of over 100 feet. Injected sparge gases traveled laterally at least 100 feet. The relatively large degree of horizontal gas movement is likely due to the heterogeneous nature of the coastal plain sediments at the site.

4.3 Mass Transfer Conceptual Models

Based on laboratory and field experiments described above and similar investigations, most current sparging literature states that sparging in predominately sandy materials will result in a steady network of individual gas channels. Since these channels have never been observed in a three dimensional field setting, and due to the fact that most natural settings are much more heterogeneous than the lab conditions where channels have been observed, others believe that infiltrating sparge gas will result in bulk desaturation similar to conditions found in the vadose zone.

As a result of this disparity, several approaches to quantifying mass transfer between the sparge gas and groundwater have developed. The approaches may be divided into three groups: classical two-phase flow, bulk equilibrium mass transfer, and channel mass transfer.

4.3.1 Classical Two-Phase Flow

As described in Chapter 3, equations describing the flow, or motion, of compounds in both the water and gas in a two-phase system are well known. If one assumes that a compound in either phase instantaneously establishes an equilibrium partitioning between the two phases when they come into contact, then the compound's Henry's law constant may be used to write the aqueous compound concentration in terms of the gaseous concentration (or vice versa):

$$C_w^j = \frac{C_g^j}{K_h^j}$$

where

C_w^j = the aqueous concentration of compound j $\left(\frac{M}{V}\right)$

C_g^j = the gaseous concentration of compound j $\left(\frac{M}{V}\right)$

K_h^j = the dimensionless Henry's law constant for compound j

This actually allows one of the governing equations to be written in terms of the other, which simplifies the resulting calculations [Binning, 1995]. If equilibrium partitioning is inappropriate, a kinetic mass transfer term must be added to each phase transport equation [Binning, 1995].

When applied to air sparging problems, classical theory predicts symmetrical, conical sparge gas distributions around the sparge well [Mohtar et al., 1994; van Dijke and van der Zee, 1994]. Natural heterogeneity ensures that this will rarely be the case. Because it assumes both phases are flowing

simultaneously in pore spaces, classical theory is inapplicable if the sparge gas flows in a network of discrete channels.

4.3.2 Bulk Equilibrium Mass Transfer

This approach was used by Wilson et al. [1992] to investigate the effectiveness of VOC removal via air stripping from a vertical, gravel-filled interception trench. As illustrated in Figure 4, a mass balance was performed on a vertical series of n rectangular cells that encompassed the entire sparge zone.

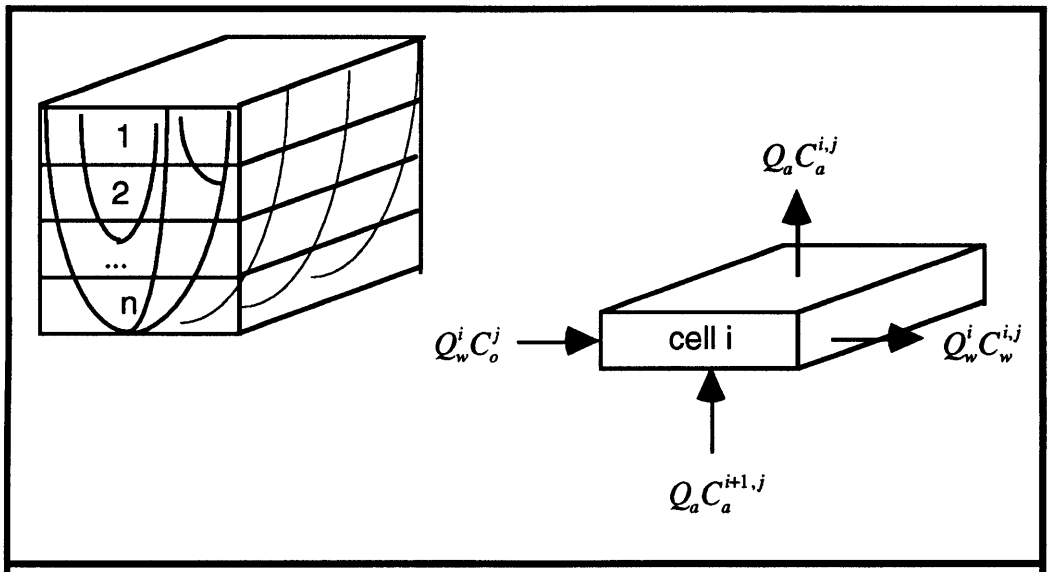

Figure 4 - Bulk Equilibrium Mass Transfer

Where

n = number of rectangular cells

Q_w^i = groundwater flow into cell i

Q_a = air flow through the sparge zone

C_o^j = initial concentration of compound j in groundwater

$C_a^{i,j}$ = air concentration of compound j in cell i

$C_w^{i,j}$ = water concentration of compound j in cell i

The hydrostatic pressure at the bottom of the *ith* cell is

$$p^i = \left(1 + \frac{z}{10.336}\right) \text{ (atm)}$$

where z is in meters measured in the downward direction from the water table and the factor of 10.336 converts meters of water to atmospheres.

The bulk flow of air through each cell increases as the pressure of the gas decreases:

$$Q_a^i = \frac{Q_a}{1 + \frac{z}{10.336}} \tag{1}$$

The mass balance for a cell i and compound j is

$$Q_w^i C_o^j + Q_a^i C_a^{i+1,j} = Q_w^i C_w^{i,j} + Q_a^i C_a^{i,j} \tag{2}$$

Substituting (1) into (2) and assuming equilibrium partitioning between phases allows one to solve for the water concentration of compound j exiting cell i as a function of depth, Henry's Law constant, initial water concentration, and water and total volumetric air flow through the sparge zone.

The mean concentration of compound j in the water exiting the sparge zone is

and the air concentration of compound *j* entering the vadose zone is simply

$$C_g^{1,j}.$$

The ability to apply this approach to sparging problems in general is limited by several underlying assumptions. The first is the assumption that the volume of sparge gas in a cell is small compared to the volume of water in the cell. As discussed in section 4.2, air saturation may reach values on the order of 40 percent in a sparge zone. At this level of air saturation, the flow of water through a cell will be reduced due to the reduction in hydraulic conductivity caused by sparging. In addition, the pressure of the gas in a cell will no longer be equal to hydrostatic pressure, since the "weight" of the water above a cell will be significantly reduced by high air saturations.

By interchanging gas and water concentrations using Henry's Law, this analysis assumes that the gas and water concentrations reach equilibrium during the residence time of the gas in each cell. This may not be a good assumption at high water and/or gas flow rates

4.3.3 Gas Channel Mass Transfer

Johnson [1994], and Mohr [1995] model the sparge zone as a uniform distribution of cylindrical air channels surrounded by a thin cylindrical zone of stagnant water. The concentration of a compound at the air/water interface and at the edge of the stagnant water zone are assumed to be constant and equal to the saturation concentration of the sparge gas at atmospheric pressure and the bulk groundwater concentration, respectively. This implies the gas concentration is uniform across the width of the gas channel, which is reasonable considering the low resistance to diffusion in gases.

Both authors estimate the mass flux per unit channel length of a given compound in and out of the channels using the solution to the diffusion equation from a uniform cylinder:

$$Q = \frac{2\pi D_w^j [C(b) - C(a)]}{\ln\left(\frac{b}{a}\right)} \left(\frac{\mathrm{M}}{\mathrm{L-T}}\right)$$

where

D_w^j = the diffusion constant of compound j in water $\left(\frac{\mathrm{L}^2}{\mathrm{T}}\right)$

b = the radial distance from the center of the channel to the stagnant boundary

a = the gas channel radius

To calculate the mass flux over the entire sparge zone, the flux per unit channel length is multiplied by the average channel length times the total number of channels.

This approach captures the essence of stable gas channel flow, but fails to take into account several factors. First is the assumption that the flux out of the channel is constant over its length. Because the concentration of a gas increases with pressure, the concentration gradient (and resulting flux) will increase with depth. Second, the diffusion coefficient of a substance in water is not strictly applicable in porous media. Finally, both Johnson [1994] and Mohr [1995] set b = 1.0 cm without any discussion. These points will be addressed in Chapter 5.

Chapter Five

Channel Mass Balance Analysis

The biozone concept is based on transporting a sufficient quantity of a compound from the ground surface into solution in a contaminated aquifer. Developing a better understanding of the way a compound dissolves into solution or evaporates out of solution is the purpose of this chapter.

The remainder of this work is based on the premise that individual sparge gas channels do form. Although this premise has not been proven, there is some evidence that it may provide the best "cartoon view" of the physical processes involved in aquifer sparging. The consequences of this premise are developed via an individual channel mass transfer conceptual model.

Consider a steady state network of cylindrical sparge gas flow channels in a phreatic aquifer and a small section of one of the channels as illustrated in Figure 5. The small representative channel element shown will be used in subsequent analysis of mass transfer in and out of the sparge channels. Several tools need to be developed before such analysis is begun.

5.1 Background Considerations

Previous work has sometimes assumed "standard" or "average" values of mass transport phenomena over the entire sparge zone. Because of the natural variability in aquifer and contamination characteristics, developing a framework to more accurately model these parameters is useful. In addition, microorganisms respond to extremely small chemical concentrations, so keeping careful track of exactly where the mass goes may be important. Because diffusion plays an important role in any liquid-gas

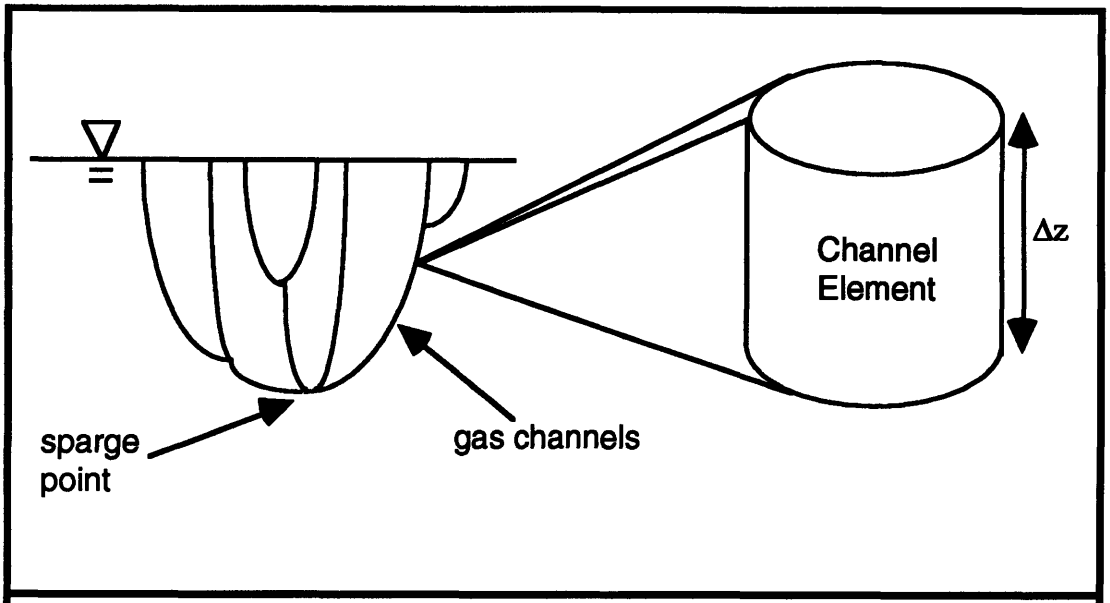

Figure 5 - Sparge Channel Network and Channel Element

mass transfer model, the molecular diffusion coefficient is considered first.

5.1.1 Molecular Diffusion

The diffusion of compound *A* through compound *B* may be thought of as the process by which molecules of *A* move via random (Brownian) motion through molecules of *B*. Physical intuition suggests that

- as the size of molecule *A* increases it will have more difficulty moving through molecules of *B*, decreasing diffusion.

- as a solution of molecules becomes more crowded, or viscous, random motion will become more challenging, decreasing diffusion.

- as temperature rises molecules of both *A* and *B* move more rapidly and are less densely packed together, increasing diffusion.

Studies confirm what intuition suggests. Schwarzenbach et al. [1993] provide the following estimate of the diffusivity of organic molecules in water:

$$D_w^j = \frac{1.326 \times 10^{-4}}{\mu^{1.14} \bullet \left(V^j\right)^{0.589}} \quad \left(\frac{cm^2}{sec}\right)$$

where

V^j = average molar volume of compound j $\left(\frac{cm^3}{mol}\right)$

μ = solution viscosity at the temperature of interest (centipoise)

This method generally yields estimates which agree with observations to within 10 percent [Schwarzenbach et al. 1993].

Molecular size may be estimated by dividing the molecular mass of the compound by its liquid density. Alternatively, estimates of diffusion volumes for several important elements are available from diffusion studies [Schwarzenbach, et al. 1993]:

Element	Volume Contribution ($cm^3 \bullet mol^{-1}$)
C	16.5
H	2.0
O	5.5
N	5.7
Cl	19.5
S	17.0
Ring Structure	-20.2

Table 1 - Diffusion Volumes

Aqueous diffusion coefficients provide valuable information regarding the diffusion of compounds in water. Applying them in porous media, however, requires further "tuning" to take into account the reduced cross section available for diffusion and the relatively tortuous path molecules must follow in pore spaces. The reduction in cross-sectional area may be estimated by the aquifer porosity (n), while a factor of 0.6 is a good estimate of the reduction in free diffusion due to movement along a tortuous path [Bear, 1972]. This gives

$$\hat{D}_w^j = 0.6 n D_w^j \left(\frac{\text{cm}^2}{\text{sec}}\right)$$

where $\hat{D}_w^j$ is the effective aqueous diffusion coefficient in porous media.

5.1.2 Gas Mixture Concentrations

The concentration of a compound in a gas mixture is usually expressed by its partial pressure. In a sparge gas mixture at a total pressure p, p^j is the partial pressure of compound j, which may be expressed as

$$p^j = x^j p$$

where x^j is the mole fraction of compound j, or the number of moles of j divided by the total number of moles present in the gas mixture.

Using the ideal gas law,

$$p^j = \frac{n^j RT}{V}$$

and the concentration of a gas compound j in moles/l is

$$C_g^j = \frac{n^j}{V} = \frac{p^j}{RT}$$

To convert to g/m^3, this concentration must be multiplied by one thousand times the molecular mass of the compound (m^j).

What is the concentration of a sparge gas compound in a channel element at a depth z below the water table? Pressure at the water table in a phreatic aquifer is, by definition, equal to 1 atmosphere (atm). The "walls" of the channel element experience a pressure equal to the weight of water above the channel element. As discussed in Chapter 3, the sparge gas must have also overcome the entry pressure in order to have invaded the pore spaces. If the entry pressure is expressed in meters of water and one defines $z' = z + p_e$, the total pressure in the channel element is

$$p(z) = 1 + 10^{-5} \rho_w g(z') \quad \text{(atm)}$$

where ρ_W is the density of water in kg/m^3 and 10^{-5} is a conversion factor between atmospheres and Pascals. The gas concentration of compound j at a depth z is therefore

$$C_g^j(z) = \frac{x^j\left(1 + 10^{-5}\rho_w g(z')\right) \bullet 1{,}000 m^j}{RT} \quad \left(\frac{\text{g}}{\text{m}^3}\right)$$

Because z decreases in the upward direction, this equation shows that the gas concentration will decrease as gas flows up towards the water table. This makes physical sense, since the gas expands as it rises in the channel and is subjected to less and less pressure from the surrounding water.

5.1.3 Gas Entry Effects

To better understand the flow of sparge gas from the ground surface into the aquifer and back up through the saturated zone, consider a vertical sparge well screened in a phreatic aquifer from a depth Z_1 to a depth Z_2 before any gas is injected:

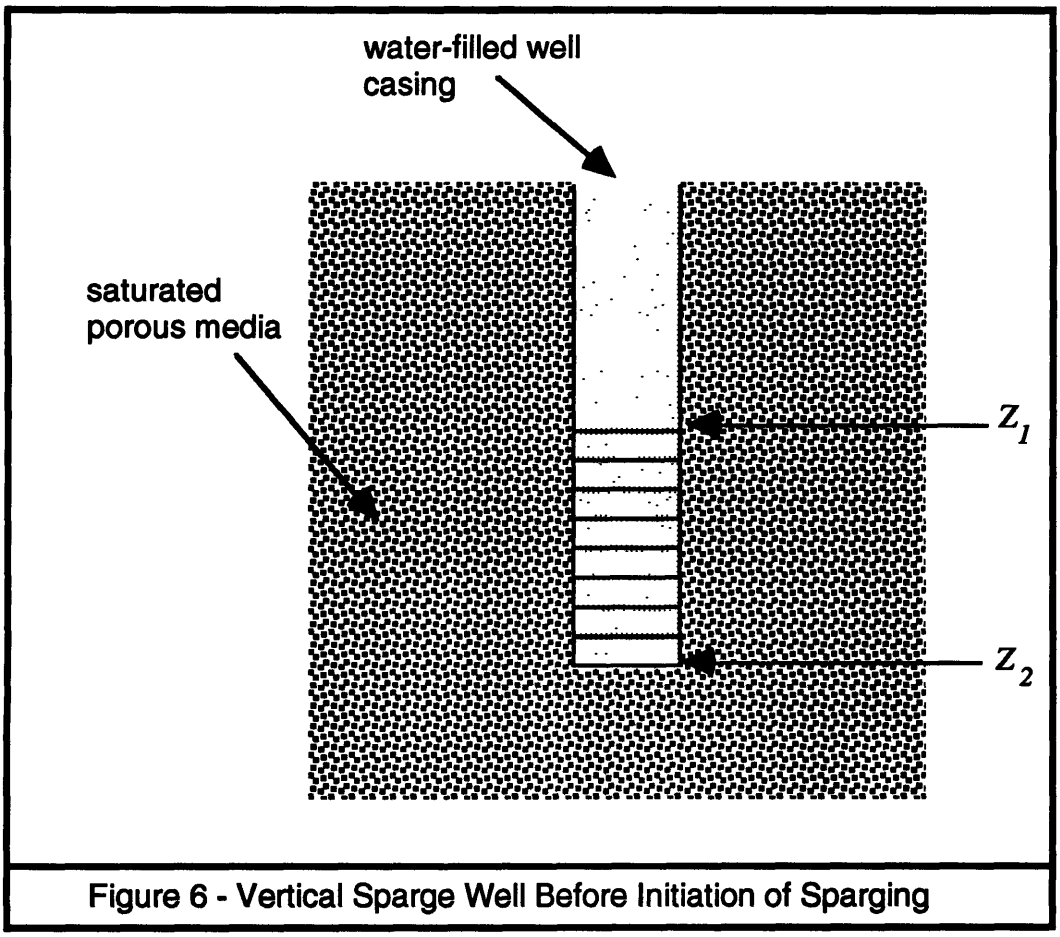

Figure 6 - Vertical Sparge Well Before Initiation of Sparging

The porous material just outside of the well screen will have a variable pore size distribution and associated variation in entry pressure. Assume the minimum entry pressure of the pores on the outside of the well screen is x cm of water.

Assume the gas injection pressure at the top of the sparge well is increased in small increments. When the sparge gas pressure reaches a value of $\rho_{wg}Z_1$, the water level in the well will be at a depth Z_1, just at the top of the well screen.

If the next incremental pressure increase is less than x cm of water, gas will continue to penetrate into the well but gas will not flow into the porous media:

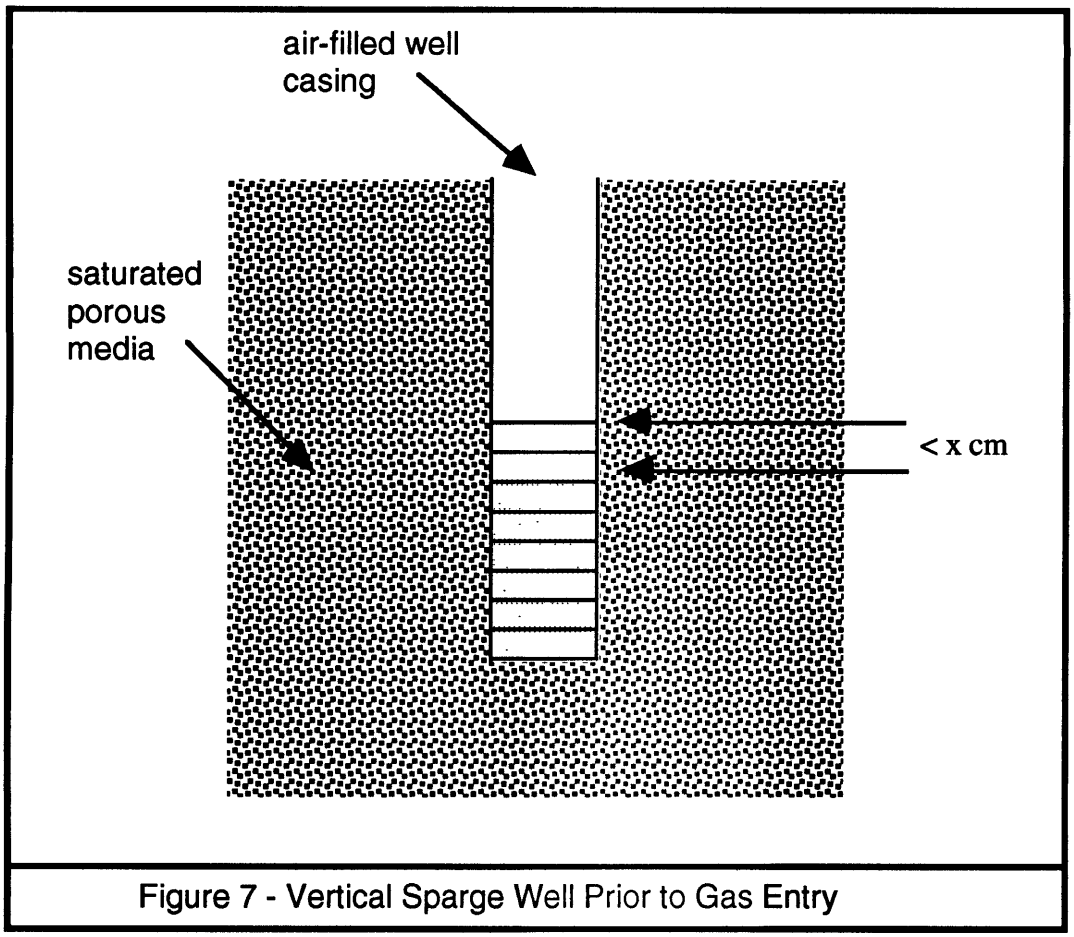

Figure 7 - Vertical Sparge Well Prior to Gas Entry

When the gas pressure is incrementally increased above Z_1 + the minimum entry pressure, gas will begin to flow into the aquifer. Since the pressure is the same everywhere in the gas, it will begin to flow radially away from the well screen under an *initially* horizontal pressure gradient. Note that if the aquifer can "accept" the air as fast as it is injected, the air will preferentially flow into the aquifer instead of further down into the well. This effect may partially explain field experiments which show sparge gases emanating only from the top of well screens [Lundegard, 1994]. If the filter pack outside the screen provides a highly permeable flowpath, sparge gas may also tend to flow up through the filter pack before entering the aquifer formation.

As injection pressure is increased, gas will preferentially enter the pores with the lowest entry pressures. This sets up a horizontal fingering effect just as the

gas exits the well screen. As soon as gas moves into the aquifer, the unstable condition of a less viscous fluid displacing a more viscous fluid exists. This type of situation also results in fingering [Ji et al., 1993]. Most importantly, the gravitational instability created by a less dense gas underlying a more dense liquid also causes a fingering of the fluid interface to occur [Bear, 1972]. There appear to be several good theoretical reasons for air channels to begin to form as sparge gas emanates from the well. Unfortunately, it is less clear that gas fingers will maintain their shape and grow into stable gas channels as they flow upward through a heterogeneous porous media.

5.2 Mass Transfer Across the Gas/Water Interface

Mass is transferred in and out of a channel element via gas flow at each end and via transfer across the gas/water interface:

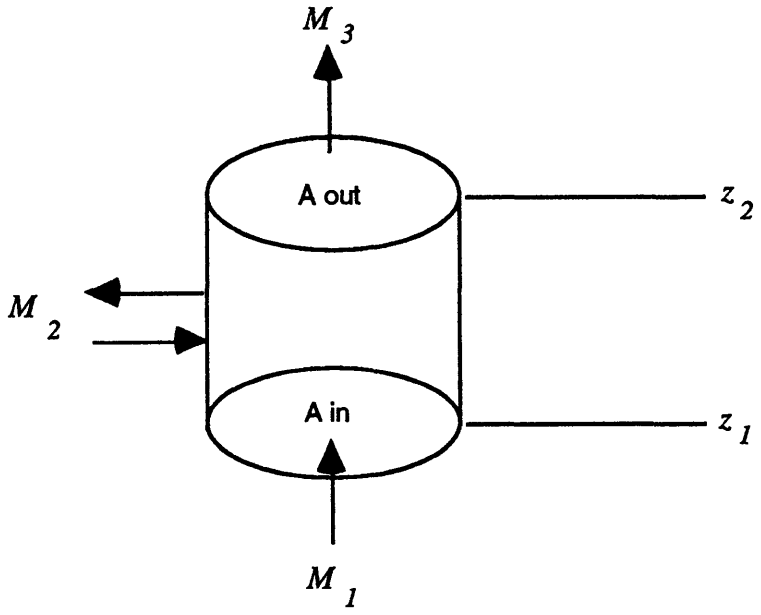

Figure 8 - Channel Element Mass Transfer

M_1 and M_3 are the fluxes into and out of the channel element; M_2 is the flux across the gas/water interface. The direction of M_2 is controlled by the concentration gradient; flux will always occur from areas of high concentration towards areas of low concentration. Adopting the convention that M_2 is positive for flow out of the channel element and assuming steady state conditions, conservation of mass requires that

$$M_3 = M_1 - M_2 \tag{3}$$

Expressing M_1 and M_3 is straightforward:

$$M_1 = Q_{in} \sum_j C_g^j(z_1) \quad \left(\frac{\mathrm{M}}{\mathrm{T}}\right) \tag{4}$$

$$M_3 = Q_{out} \sum_j C_g^j(z_2) \quad \left(\frac{\mathrm{M}}{\mathrm{T}}\right) \tag{5}$$

where Q_{in} and Q_{out} are the volumetric gas flows (L^3/T) entering the bottom and exiting the top of the channel element. Transport due to axial (longitudinal) dispersion is assumed to be negligible in comparison to the advective transport represented in equations (4) and (5).

The solution to constant radial diffusion presented in section 4.3.3 will be used to determine M_2:

$$Q = \frac{2\pi D[C(b) - C(a)]}{\ln\left(\frac{b}{a}\right)} \quad \left(\frac{\mathrm{M}}{\mathrm{L\text{-}T}}\right) \tag{6}$$

The concentration at a, the gas/water interface, may be expressed as mass per volume water through the use of Henry's Law:

$$C(a) = \frac{C_g^j}{K_h^j} = \hat{C}_g^j$$

Rewriting (5) using the notation developed thus far and multiplying by the length of a channel element gives

$$M_2^j = \frac{2\pi \hat{D}_w^j \left[C_w^j(b) - \hat{C}_g^j(z) \right] \Delta z}{\ln\left(\frac{b}{a}\right)} \left(\frac{\text{g}}{\text{sec}}\right) \tag{7}$$

Substituting (4), (5), and (7) into (3) gives

$$Q_{out} \sum_j C_g^j(z) = Q_{in} \sum_j C_g^j(z + \Delta z) - \frac{2\pi \hat{D}_w^j \left[C_w^j(b) - \hat{C}_g^j(z) \right] \Delta z}{\ln\left(\frac{b}{a}\right)} \tag{8}$$

$$M_3 \quad = \quad M_1 \quad - \quad M_2$$

To use this equation, one must estimate a characteristic distance, b, at which the water concentration will be maintained at some constant value. To determine this distance, the relative importance of competing transport mechanisms must be assessed.

Before further investigating the flux across the wall of the channel element, an observation may be made about variation in the channel shape. Without any mass transfer across the gas/water interface, the mass entering the bottom of the channel element must equal the mass exiting the top:

$$Q_{in} \sum_j C_g^j(z_1) = Q_{out} \sum_j C_g^j(z_2)$$

$$M_1 \quad = \quad M_3$$

The volumetric flow of gas into a channel element equals the velocity of the gas times the cross-sectional area through which it passes. Because the channel element is in a porous media, its effective cross-sectional area is

reduced by (approximately) the porosity, while the velocity is equal to the specific discharge divided by the porosity:

$$v_g A_{eff} = \frac{q_g}{n} \bullet A\, n = q_g A$$

where

v_g = the velocity of the gas in the channel element

A_{eff} = the effective cross-sectional area of the channel element

q_g = specific discharge of sparge gas through the channel element

n = aquifer porosity

A = the cross-sectional area of the channel element

With this stipulation, consider the relationship between the volumetric gas flow rate of a pure gas in and out of a channel element:

$$\frac{v_{g_{out}} A_{out}}{v_{g_{in}} A_{in}} = \frac{C_g^j(z_1)}{C_g^j(z_2)}$$

$$= \frac{\dfrac{x^j\left(1+10^{-5}\rho_w g(z_1)\right) \bullet 1{,}000MW}{RT}}{\dfrac{x^j\left(1+10^{-5}\rho_w g z_2\right) \bullet 1{,}000MW}{RT}}$$

$$= \frac{1+10^{-5}\rho_w g(z_1)}{1+10^{-5}\rho_w g(z_2)}$$

Since z_1 is greater than z_2, more cubic feet of gas per unit time exit the top of the channel element than enter the bottom. For this to be the case, either the gas must speed up, the diameter of the channel must increase, or some combination of the two must occur.

No lab or field studies have investigated variation in gas velocities or channel diameters. Authors usually assume a constant velocity or a constant diameter, although at least one author assumes both to be true [Acomb et al., 1995]. The magnitude of this effect can be estimated, however.

Sparge depths are usually on the order of 10 to 100 feet below the water table, with the vast majority using injection depths of less than 40 feet [API, 1995]. For a sparge depth z, an initial channel radius of r_{in}, and a constant gas velocity, the radius of the channel at the water table may be calculated by:

$$r_{out} = \left(\frac{1 + 10^{-5} \rho_w g z}{1} (r_{in})^2 \right)^{1/2}$$

For instance, an initial channel radius of 2 mm at a sparge depth of 40 feet will grow to almost 3 mm at the water table. Similarly, if the channel diameter is held constant and specific discharge is allowed to vary, the percent increases in v_{out} versus v_{in} will be the same. If the net flux of gas out of the channel across the gas/water interface is large enough, this trend may be reversed and the channel may collapse.

What would one expect the velocity of the gas flowing upward in the channel to be? At some distance from the sparge point the motion of the gas will be dominated by the pressure gradient along its length as opposed to the pressure applied by the compressor. Using the Darcy equation for gas flow and assuming $k_g = 1$,

$$\vec{q}_g = -\frac{k}{\mu_g} \left(\nabla p_g - \rho_g \vec{g} \right)$$

Assuming gas is flowing only in the z direction,

$$q_g = -\frac{k}{\mu_g} \left(\frac{dp_g}{dz} - \rho_g g \right)$$

Assuming hydrostatic conditions in the water and that the vertical pressure gradient in the air is the same as that in the water,

$$\frac{dp_g}{dz} = \rho_w g$$

Noting that

$$\rho_w g >> \rho_g g$$

gives

$$q_g = -\frac{k\rho_w g}{\mu_g}$$

Expressing k in terms of the vertical hydraulic conductivity of water

$$K_z = \frac{k\rho_w g}{\mu_w}$$

gives

$$q_g = -K_z \frac{\mu_w}{\mu_g} \qquad (9)$$

Because z increases in the downward direction, a negative value of q_g represents upward flow.

Both the viscosity of water and the viscosity of gases at low densities do not vary much over several atmospheres [CRC, 1993]. Assuming a horizontal hydraulic conductivity of water equal to 100 m/day and an hydraulic conductivity anisotropy ratio of 10:1, a reasonable vertical hydraulic conductivity of would be 10 m/day. Using the viscocities of air and water at 1 atm and 20 °C (0.01813 centipoise and 1.0019 centipoise, respectively), results in a gas specific discharge in a channel element on the order of 500 m/day or 0.6 cm/sec. Dividing by an effective porosity of 0.25 gives a gas

velocity of 2.4 cm/sec. This value will be compared to estimated gas velocities in the case study described in Chapter 6.

5.2.1 Relative Importance of Diffusion and Advection

The characteristic transport time for diffusion to occur over a distance l is

$$t_{diffusion} \approx \frac{l^2}{2D}$$

while the time for horizontal advection transport over the same distance is

$$t_{advection} = \frac{l}{v_s}$$

The transition distance where diffusive and advective mass transport are of approximately equal importance is found by setting the transport times equal to one another and solving for l.

$$l_t \approx \frac{2D}{v_s}$$

Typical values for D_w are on the order of 10^{-5} to 10^{-6} cm^2/sec. Groundwater seepage velocities for relatively porous aquifers may be on the order of m/day, resulting in transition lengths on the order of 0.1 mm to 0.01 mm. Figure 9 uses a hypothetical cylindrical sparge gas channel to illustrate the "competition" between diffusive and advective transport.

Consider molecule **1**, which has just left the gas channel. Due to random molecular motion, it is being "driven" outward radially by diffusion in the direction of the concentration gradient. Although the water in which it now exists may be moving, it *appears* stagnant compared to the speed at which **1** is moving due to diffusion. As the molecule moves to a distance l_t, its motion begins to become dominated by advection. A concentration gradient still exists, so the molecule is still diffusing. But the *relative* effect of diffusion

becomes small and the molecule follow a path represented by molecule **2** (the transition from diffusive to advective transport is not as abrupt in nature as is shown in Figure 9). Similarly, the motion of molecule **3** is affected by a

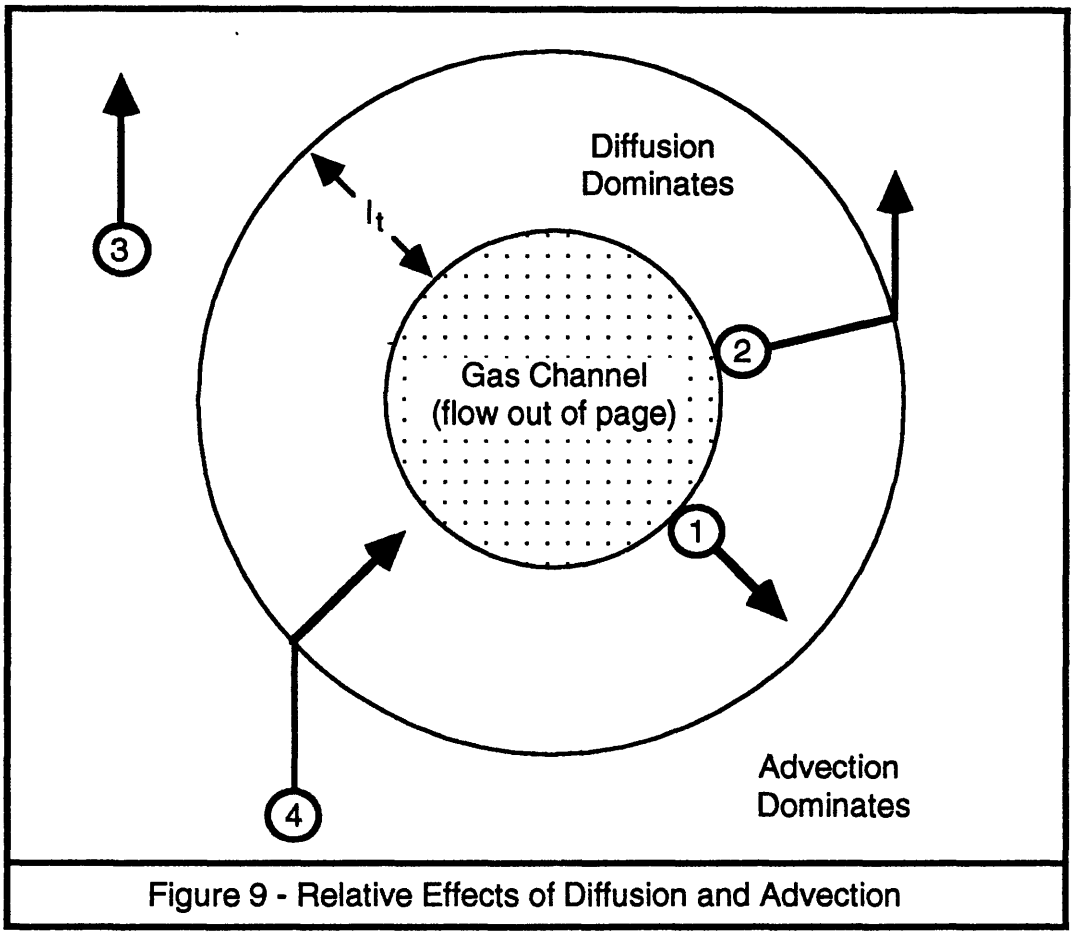

Figure 9 - Relative Effects of Diffusion and Advection

diffusive gradient towards the gas channel but dominated by advection. Molecule **4** has made the "transition" from advective to diffusive transport as it moved within a distance l_t.

The stagnant film around a channel will not actually be of uniform thickness. The flow of water past the channel will create a wake effect, with a thinner stagnant layer on the upgradient side of the channel and a thicker layer on the downgradient side. Diffusion across the layer will vary accordingly. The use

of a single thickness for the stagnant boundary layer represents an "averaging" of the actual layer thickness.

Values for all the variables in (8) are able to be calculated or estimated at this point. The following steps may be used to perform the mass balance on each channel element in a representative channel in a sparge zone:

1. Estimate the number of channels receiving output from sparge well.

2. Calculate the volumetric gas flow into each channel.

3. Calculate gas concentration of each compound in the sparge gas at the sparge depth.

4. Calculate the mass flux of each compound entering the channel element.

   This flux is equal to the flow rate calculated in Step 2 times the concentration calculated in Step 3.

5. Calculate the mass flux across the channel element wall for both sparge gas compounds and groundwater contaminants using

$$M_2^j = \frac{2\pi \hat{D}_w^j \left[C_w^j(b) - \hat{C}_g^j(z') \right] \Delta z}{\ln\left(\frac{b}{a}\right)}$$

6. Calculate the mass flux exiting the channel element for all compounds

$$M_3^j = M_1^j - M_2^j$$

   Note that this is the entering flux for the next channel element in series.

7. Calculate the mole fraction of each compound in the gas mixture entering the next channel element.

8. Repeat steps for the next channel element beginning at Step 3.

Calculating mass transfer in discrete steps allows a more detailed understanding of the sparging process. The sequential mass balance methodology outlined in Steps 1-8 above are applied to a case study in Chapter 6. Additional effects of sparging are considered first.

5.3 Secondary Effects of Sparging

5.3.1 Reduction in Hydraulic Conductivity

Consider a number of vertical, cylindrical channels with radius r distributed in aligned rows perpendicular to the direction of groundwater flow. If D is the distance between the center of air channels, the number of channels per unit area in the x-y plane is $(1/D)^2$ and the number of channels per unit length is $1/D$.

The air saturation, or percentage of the bulk aquifer volume occupied by air channels, is equivalent to the percentage of x-y plane surface area occupied by the channels:

$$S_a = \frac{\pi r^2}{D^2}$$

A rough estimate of the reduction in horizontal hydraulic conductivity due to channel formation is the reduction in y-z plane surface area available for the groundwater to flow through. This is equivalent to the percentage of linear distance encompassed by the channels:

$$\frac{K_{sparge}}{K_r} = \left(1 - \frac{2r}{D}\right)$$

where K_r is the radial or horizontal hydraulic conductivity and K_{sparge} is the reduced hydraulic conductivity in the sparge zone. Literature estimates of channel radius are on the order of several pore sizes, or millimeters [Johnson, 1994]. Estimates of average channel spacing vary from 0.1 m to 1.0 m [Johnson, 1994]. Values in these ranges may be used to evaluate the magnitude of potential air saturations and reductions in hydraulic conductivity caused by sparging.

r (mm)	D (mm)	% air saturation	% K reduction
0.5	1,000	7.85e-7	0.001
2.5	1,000	1.95e-5	0.005
0.5	10	0.00785	0.1
2.5	10	0.19	0.5

Table 2 - Changes in Air Saturation and Hydraulic Conductivity

A significant reduction in conductivity will only occur for channels spaced relatively close together. The reduction in hydraulic conductivity has the potential to significantly impact the direction of groundwater (and therefore plume water) flow.

5.3.2 Plume Deflection

The possible magnitude of change in groundwater flow direction was investigated using the MacPoisson™ software program [Cooke et al., 1989]. This program utilizes finite element analysis to calculate the solution to Poisson's equation for a variety of user-defined boundary conditions.

An unconfined aquifer approximately 150 feet thick was used for this section of the study. The bottom of the aquifer and the water table were set as no-flow boundaries and linear head change of 1.5 feet was imposed across a 900

foot-long cross section in the x - z plane, resulting in a horizontal hydraulic gradient of 0.00167. The sparge depth was 130 feet and the sparge zone was 180 feet wide. Based on a horizontal to vertical hydraulic conductivity ratio of 10 to 1, an equivalent isotropic system requires a horizontal axis compression of approximately 3 to 1. Figure 10 shows the triangular finite element mesh and the boundaries of the sparge zone.

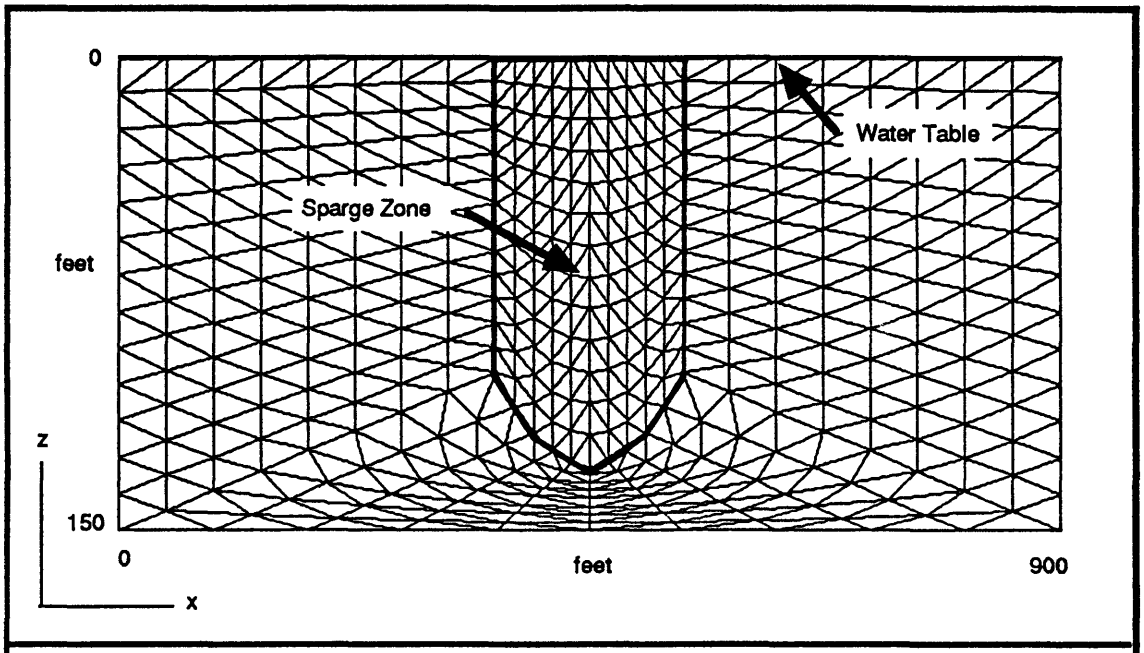

Figure 10 - Finite Element Mesh

Based on the boundary conditions described above, and setting the hydraulic conductivity in the sparge zone equal to 33 percent of the conductivity in the aquifer, a set of isopotential head lines was generated, as shown in Figure 11.

Finally, flow lines were drawn perpendicular to the isopotential lines to evaluate the approximate magnitude of plume deflection caused by sparging. As shown in Figure 12, the flow lines indicate a minimum distance beneath the plume at which the sparge point must be located to prevent the plume from partially flowing under the sparge zone. In the illustrated case, the sparge

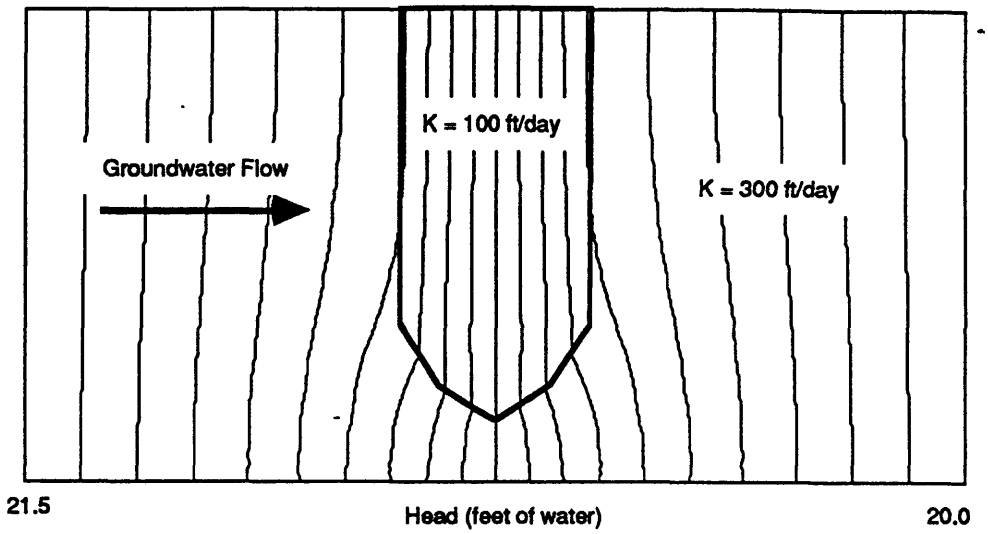

Figure 11 - Isopotential Head Lines

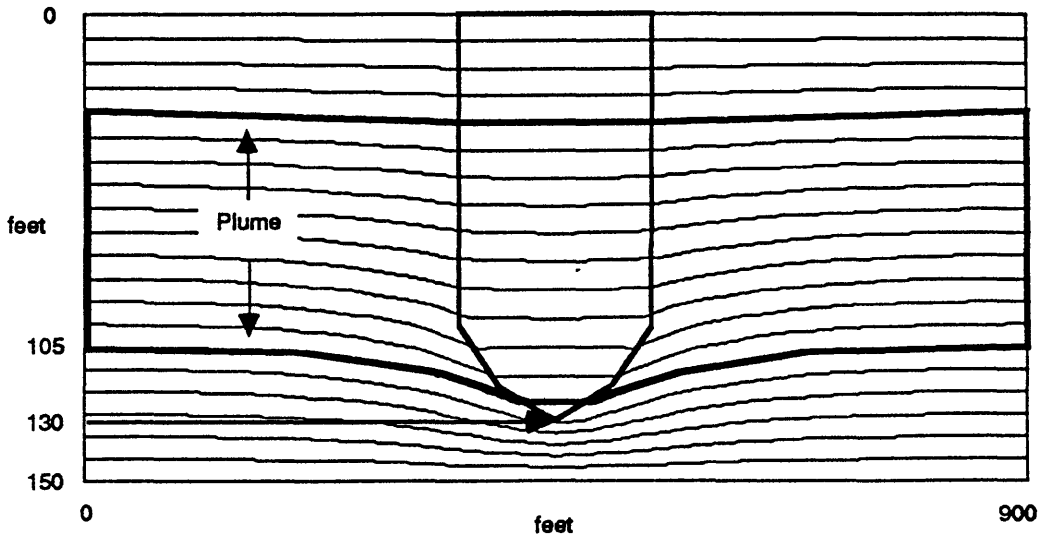

Figure 12 - Flow Lines Showing Plume Deflection

point must be located approximately 25 feet below the bottom of the hypothetical plume.

5.3.3 Geochemical Effects

The benefits of injecting oxygen into an aquifer to stimulate biotransformation of contaminants may also change the redox potential of an aquatic system. Increased oxygen levels may result in precipitation of iron oxyhydroxides or other metal precipitates [API, 1995]. Significant precipitation may clog aquifer pores, reducing hydraulic conductivity. More frequently, precipitation concentrates at the injection point and clogs the well screen. The magnitude of this effect will depend on the unique chemical environment (pH, Eh, dissolved metal concentrations) of the aquifer system and must be evaluated on a site-specific basis.

5.3.4 Biofouling

The stimulation of too much microbial biomass may also begin to clog pore spaces or well screens. One method used to minimize this effect is to inject compounds required for bioremediation out of sequence with one another. The compounds will eventually mix as they disperse through the aquifer, but only microorganisms away from the well screen will be stimulated [Semprini et al., 1992].

Chapter Six

Case Study: Plume LF-1

One of the major goals of this work is to evaluate the feasibility of the biozone concept in a "real-world" scenario. A case study serves to illustrate the theoretical concepts developed in Chapter 5 and to test the practical outcome of that theory. A plume known as the "LF-1 plume" will be used for the case study.

6.1 Introduction

The contamination source for this plume is the site of a former landfill on the Massachusetts Military Reservation (MMR), which is located on the western portion of Cape Cod, Massachusetts. The geologic, hydrogeologic, and contamination data presented in this chapter were obtained from an investigation perfumed under the auspices of the Installation Restoration Program at the MMR [CDM, 1995]. Figure 13 shows the approximate location of the MMR.

A variety of military and government tenants have occupied portions of the MMR during its 84 year history, including the U. S. Army, Navy, Air Force, Air National Guard, and Coast Guard. The landfill operated from 1941 to 1989 as the primary solid waste disposal facility at the MMR. Disposal activities during the majority of this time were unregulated, and accurate records describing waste types and quantities do not exist. Wastes that may have been placed in the landfill include general refuse, fuel tank sludge, solvents, herbicides, transformer oil, paint, DDT powder, blank small arms ammunition, and live ordnance. Investigations indicate that waste was usually buried in linear

trenches and covered with soil on a daily basis. The landfill covers approximately 100 acres.

Investigations discovered soil contamination at the landfill site and groundwater contamination in the unconfined aquifer below the site. To minimize further transport of landfill source materials into underlying groundwater, the most heavily contaminated portions of the landfill source area were covered with a multi-layer synthetic cap in 1993 and 1994. The remainder of the source area is covered by a maintained vegetative cover.

The western edge of Cape Cod encompasses three major water-bearing geologic deposits. The landfill itself lies in the Mashpee Pitted Plain (MPP), and the Buzzards Bay Moraine (BBM) lies to the immediate west. The Buzzards Bay Outwash (BBO) deposit lies still further to the west and continues to Buzzards Bay. Groundwater beneath the landfill flows to the southwest and west through the three deposits in sequence. The approximate boundaries of the MPP, BBM, and BBO are shown in Figure 13.

The MPP and the BBO are outwash plains composed of sediments deposited during the recession of the Wisconsinian glacier. The sediments are heterogeneous, composed mostly of alternating layers of coarse, medium, and fine sand. Local, discontinuous intervals of gravel and fine grained materials (i. e. silts, clays) exist throughout both deposits.

The BBM was formed by the furthest southern advance of a lobe of the Wisconsinian glacier. Geologic investigations indicate that tectonic processes may also be responsible for the structure of the moraine. BBM material is very heterogeneous, varying from well-sorted coarse sand and gravel to dense, very poorly sorted fine to coarse sand, gravel, silt and clay. In general, investigations indicate that the BBM is composed of finer, more poorly sorted material than the MPP or BBO.

All three formations are underlain by impermeable deposits which form the lower boundary of an unconfined aquifer system. The BBM is underlain by a

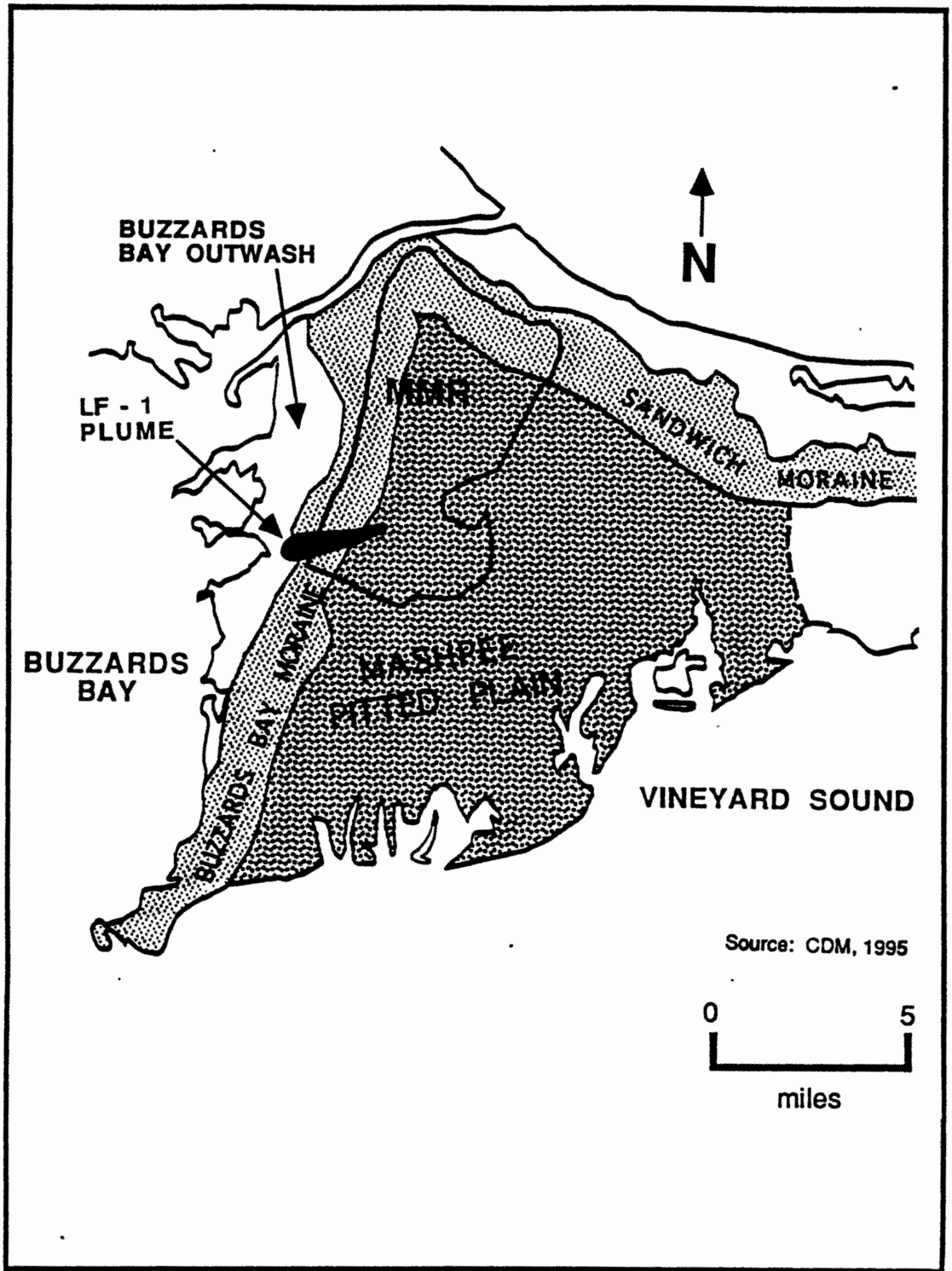

Figure 13 - MMR, Geologic Formations, and Plume LF-1

relatively thin layer of laminated silts, clays and fine sands of glacio-lacustrine origin. To the west, the base of the aquifer is bedrock or bedrock overlain by a thin layer of basal or lodgment glacial till. Groundwater altitudes vary from a high of approximately 65 feet above mean sea level (MSL) at the source area to a low of approximately 25 feet above MSL at the western edge of the LF-1 plume. The base of the aquifer is encountered at approximately 130 feet below MSL, resulting in an aquifer thickness of approximately 150 feet at the leading edge of the plume.

Groundwater in the vicinity and downgradient of the former landfill is contaminated with a variety of compounds, including chlorinated solvents, aromatic hydrocarbons, and inorganic cations. TCE and perchloroethylene (PCE) exceed their groundwater maximum contaminant levels (MCL) of 5 micrograms per liter (μg/l) throughout a large percentage of the plume. The maximum concentrations of PCE and TCE are 68 μg/l and 64 μg/l, respectively.

Available data indicate that the LF-1 VOC plume is roughly elliptical in shape, with a thickness that varies between approximately 30 to 120 feet. The plume is approximately 16,000 feet long and 6,000 feet wide at its longest and widest. The approximate location of the LF-1 plume is shown in Figure 13.

6.2 Feasibility Evaluation

In this section, the channel element mass balance approach developed in Chapter 5 will be used to evaluate the feasibility of using the biozone to remediate the TCE in the LF-1 plume.

For the purposes of this case study, it will be assumed that

1. Methanotrophic bacteria capable of aerobically oxidizing TCE exist in the aquifer and biotransformation is not limited by nutrient concentrations.

2. The groundwater TCE concentration must be reduced to below the MCL of 5 μg/l.

3. Sparge gas is injected via a single horizontal well running perpendicular to the major plume axis.

4. Gas is injected at a depth of 30 meters below the water table and results in a biozone thickness of 60 meters.

5. The initial radius of gas channels at a depth of 30 meters is 2 mm and the average channel density is 1 channel per square meter.

Assumption #4 is based on an air sparging pilot test performed in the MPP deposit, which has geologic properties similar to the BBO [Advanced Sciences, 1994]. During the pilot test, air was injected at 125 cfm at a depth of approximately 20 meters below the water table. The maximum radial distance affected by sparging was measured by a variety of methods, including dissolved oxygen concentration and sodium hexaflouride gas tracer. The maximum radial distance measured was approximately 30 meters. If this figure were applied directly to a horizontal well at a sparge depth of 20 meters below the water table, one would predict a biozone thickness of 60 meters. At the hypothetically sparge depth of 30 meters, a slightly larger zone of influence would be expected. Thus, assumption #4 is relatively conservative.

Assumption #5 is also conservative, as the channel size and channel density are both towards the low end of values quoted in sparging literature.

For the biozone to be successful, it must be able to accept a continuous introduction of the maximum contaminant concentration. A conservative value of 70 μg/l will therefore be used for both contaminants in the calculations below. The plume will be treated as a rectangular slab with dimensions

Length (m):	5,000
Width (m):	2,000
Thickness (m):	30

(The LF-1 plume dimensions are approximately proportional to a stack of sixteen 8.5" x 11" sheets of paper cut in half lengthwise.)

Hydrogeologic data for the LF-1 plume are summarized by CDM [1995]. Slug test estimates of hydraulic conductivity in the BBO varied over three orders of magnitude, from values on the order of one to several hundred feet per day. A pump test performed near the leading edge of the plume indicates that a horizontal hydraulic conductivity value of approximately 300 ft/day or 100 m/day is appropriate for this portion of Cape Cod. A horizontal hydraulic gradient (J) of 0.00682 was determined from water altitude measurements in BBO monitoring wells. The effective porosity in the BBO was analyzed using grain size analysis and inspection of soil types. Both methods gave values of approximately 0.23. A value of 0.25 will be used in the calculations below.

The criteria listed in Chapter 1 must hold if the biozone concept is to successfully remediate the LF-1 plume:

1. The time spent by the plume in the biozone must be sufficient to allow biodegradation to reduce contaminant concentrations below regulatory limits.

2 Sparging must transfer a sufficient mass of the necessary biological components into solution to allow for continuous biodegradation of the maximum plume concentration.

3. Sparge gas exiting the top of the biozone must not transport a mass of contaminant to the atmosphere at concentrations that exceed regulatory limits.

4. Changes in hydraulic conductivity caused by sparging must not cause the plume to flow around or under the biozone.

An approximate evaluation of the fourth condition may be made at this point. Using the relationship developed in section 5.3.1 to calculate the reduced horizontal hydraulic conductivity caused by sparging gives

$$\frac{K_{sparge}}{K_r} = 1 - \frac{2r}{D} = 1 - \frac{2 \bullet 0.002}{1} = 1 - 0.004 = 0.996$$

This results in a reduction in K_r from 300 ft/day to 298.8 ft/day. As discussed in section 5.3.2, this small reduction in hydraulic conductivity will not result in significant deflection of the plume, and the fourth condition is met. To test conditions #1 through #3, the mass transfer of compounds in and out of the LF-1 plume must be determined.

6.2.1 Channel Element Mass Transfer

The mass balance on a series of channel elements may now be calculated. The repetitive nature of the mass balance process lends itself to calculation via spreadsheet or computer program. Spreadsheet calculations for the case study are presented in Appendix A. A "walk through" of the mass balance calculation steps for the deepest channel element is presented here. The channel element length was set to 1 meter and the groundwater temperature was set to 10 °C (close to the mean annual air temperature for this region). The first step is to calculate constants.

For the compounds of interest at 10 °C:

$$V^{PCE} = 2(C) + 4(Cl) = 2(16.5) + 4(19.5)$$

$$= 111 \ \frac{cm^3}{mol}$$

$$V^{TCE} = 2(C) + 3(Cl) + 1(H) = 2(16.5) + 3(19.5) + 1(2.0)$$

$$= 93.5 \ \frac{cm^3}{mol}$$

$$D_w^{PCE} = \frac{1.326\times10^{-4}}{1.307^{1.14}\bullet(111)^{0.589}} = 6.099\times10^{-6}\ \frac{cm^2}{sec}$$

$$D_w^{TCE} = \frac{1.326\times10^{-4}}{1.307^{1.14}\bullet(93.5)^{0.589}} = 6.748\times10^{-6}\ \frac{cm^2}{sec}$$

$$\hat{D}_w^{PCE} = n\tau D_w^{PCE} = 0.25\bullet0.6\bullet D_w^{PCE} = 9.15\times10^{-7}\ \frac{cm^2}{sec}$$

$$\hat{D}_w^{TCE} = n\tau D_w^{TCE} = 0.25\bullet0.6\bullet D_w^{TCE} = 1.01\times10^{-6}\ \frac{cm^2}{sec}$$

The constants for oxygen, nitrogen, and methane are given in Appendix A.

1. Estimate number of channels receiving output from sparge well.

   The total surface area encompassed by the biozone is approximately 2,000 m (well length) times 60 m (biozone width) or 120,000 m^2. A channel density of 1 channel/m^2 results in a total of 120,000 channels.

2. Calculate the volumetric gas flow into each channel.

   No data exists on the use of a horizontal sparging well several thousand feet in length, so an appropriate volumetric flow rate is difficult to estimate.

   The pilot test conducted in the MPP [Advanced Sciences, 1994] used a fairly high (125 cfm) flow rate to maximize volatilization. Assuming a channel density of 9 channels/m^2, a total of approximately 26,000 channels would have received an average of 0.005 cfm per channel. For the 120,000 channels in the case study to receive the same volumetric flow, a 600 cfm compressor capable of pumping at a pressure of 60 pounds per square inch is required. In practice,

compressor limitations may require more than one horizontal well to be built. For the purposes of the case study, a single well and 600 cfm compressor will be assumed.

3. Calculate gas concentration of each compound in sparge gas at the sparge depth.

   These concentrations are presented in Appendix A. The initial composition of the sparge gas was set at 4 percent methane (by volume) in air. A higher methane concentration would be advantageous, but the lower explosive limit for methane is 5 percent by volume. The formula for the gas concentration of component j is

$$C_g^j(z) = \frac{x^j\left(1+10^{-5}\rho_w g(z')\right) \bullet 1{,}000 m^j}{RT}$$

   For the relatively porous material in the BBO, a minimum entry pressure of 0.2 m of water was used to calculate partial pressures.

   Note that nitrogen is included in the mass balance calculations not because its flux is important to bioremediation but because it accounts for such a large percentage of the mass flow in each channel. To be completely precise, a term for each compound in the groundwater with an appreciable ability to partition across the gas/water interface should be included. In practice, oxygen and nitrogen will dominate the mass flow when air is used as a carrier gas for methane.

4. Calculate the mass flux of each compound entering the channel element.

   This flux is equal to the flow rate calculated in Step 2 times the concentration calculated in Step 3. Results are given in Appendix A.

5. Calculate the mass flux across the channel element wall for both sparge gas compounds and groundwater contaminants using

$$M_2^j = \frac{2\pi D_w^j \left[C_w^j(b) - \hat{C}_g^j(z') \right] \Delta z}{\ln\left(\frac{b}{a}\right)}$$

The value of b is equal to $a + l_t$. As discussed in 5.2.1, the value of l_t may be on the order of 0.01 to 0.1 mm. To be conservative, a value of 0.1 mm will be used.

6. Calculate the mass flux exiting the channel element for all compounds

$$M_3^j = M_1^j - M_2^j$$

Note that this is the entering flux for the next channel element in series.

6.2.2 Results and Sensitivity Analysis

As shown in Appendix A, the channel element mass balance method provides the mass flux of each compound into or out of each channel element. The total flux into or out of groundwater for a single channel is the sum of the individual channel element fluxes, and the sum of all the channel fluxes is the total flux into or out of the biozone.

The third criteria for success depends on the flux of PCE and TCE to the atmosphere from the vadose zone. The flux to the vadose zone due to sparging is equal to the flux out of the top of the uppermost channel element in an average channel times the number of channels. Making the conservative assumption that the flux to the atmosphere is equal to the flux to the vadose zone, the flux per square meter of ground surface may then be determined by dividing by the surface area encompassed by the biozone. Using channel element #1 flux values from Appendix A results in a flux to the atmosphere of approximately 2×10^{-8} g - sec^{-1} - m^{-2} for both TCE and PCE. This flux should not result in an air concentration above U.S. EPA preliminary remediation goal standards, which are on the order of 10^{-6} g/m^3.

Conditions #1 and #2 are the most challenging. To evaluate condition #1, the plume's residence time in the biozone must be calculated. Assuming advection is the dominant transport mechanism over horizontal distances on the scale of the width of the biozone (60 m), the minimum residence time of a contaminant in the biozone is

$$t_{res} = \frac{W_{bio}}{v_s}$$

where W_{bio} is the width of the biozone and v_S is the seepage velocity

$$v_s = \frac{q_x}{n_e} = \frac{K_{sparge} J}{n_e}$$

Using LF-1 parameters results in a seepage velocity of 2.7 m/day and a minimum residence time of 22 days.

Is 22 days enough time for TCE contamination to be reduced to below the MCL? The total flux into or out of the biozone is the average channel flux times the number of channels in the biozone. Total delivery of oxygen and methane into groundwater in the biozone for the test case were approximately 2.3×10^5 g/day and 1.7×10^4 g/day, respectively.

To evaluate biotransformation of TCE in the LF-1 plume, the biozone will be treated as a large bioreactor with lumped (average) parameters. The steady state aqueous methane and oxygen concentrations in the biozone may then be estimated by dividing their total addition rate by the volumetric addition rate of water into the biozone:

$$C_w = \frac{M_{total}}{Q_w} = \frac{M_{total}}{K_{sparge} J A_{bio}} \left(\frac{g}{m^3}\right)$$

where A_{bio} is the cross-sectional area of the biozone though which water flows horizontally. For the LF-1 plume, the resulting methane and oxygen

concentrations were approximately 0.46 g/m^3 and 6.2 g/m^3, respectively. Field and laboratory studies indicate that approximately 2.5 g of oxygen are required to oxidize one gram of methane [Semprini et. al., 1990], so methane will be limiting in this case.

The methane is utilized by methanotrophic bacteria as an energy source, resulting in a steady concentration of methanotrophs in the biozone. Typical cell yields for methanotrophs are on the order of 0.8 g cells/g methane [Semprini et al., 1994], which results in a steady methanotroph concentration of 0.37 g cells/m^3 water.

At low secondary substrate (TCE) concentrations, the rate of substrate consumption may be approximated by a pseudo-first order decay:

$$\frac{d[TCE]}{dt} = -k_{bio}[\text{TCE}]$$

where

$$k_{bio} = k'\left(\frac{\text{g cells}}{\text{m}^3}\right)$$

Field-applicable values of k', which is actually the ratio of two constants used to describe biotransformations when a steady-state biomass exists, are not known with certainty. Semprini et al. [1992] use a value of 0.01 m^3 - g^{-1} - day^{-1} for TCE and a value of 2.0 m^3 - g^{-1} - day^{-1} for methane. Wackett [1995] reports values for TCE on the same order as methane based on lab studies. An intermediate value of 0.1 m^3 - g^{-1} - day^{-1} will be used here, resulting in a k_{bio} of 0.037 day^{-1}.

Recalling the retention time in the biozone is 22 days, the concentration of TCE exiting the biozone may be calculated:

$$[TCE]_{out} = [TCE]_{in} e^{-k_{bio} t}$$

$$= 31 \frac{\mu g}{l}$$

This is well above the MCL of 5 µg/l, and the biozone concept fails to remediate the plume.

A significant (> 50%) reduction in TCE concentration did occur, however. Numerous conservative assumptions were made to arrive at this result, including neglecting the removal of TCE via volatilization, the seepage velocity retardation factor due to adsorption, and the low channel density. It is interesting to note that significant biotransformation occurred in the test case even at average dissolved oxygen levels well below saturation (6.24 g/m^3).

The channel size and spacing used in the LF-1 case study were conservative values chosen from published ranges based on laboratory experiments. Current understanding of gas flow does not allow the size and spacing of channels to be calculated, but the calculation of gas velocity described in section 5.2 may offer some insight into reasonable values.

In the case study, a volumetric gas flow per channel of 0.005 cfm (2.4×10^{-6} m^3/sec) was assumed. This flow was assumed to pass through an effective cross sectional area of a cylinder with a radius of 2 mm in a medium with a porosity of 0.25, or an area of 3.14×10^{-6} m^2. The gas must therefore enter the cylinder at a velocity of 76 cm/sec, which is an order of magnitude higher than the velocity of 2.4 cm/sec estimated in section 5.2 using the Darcy equation.

There are two ways to achieve an apparent velocity on the order of 2 cm/sec. Either the size of the channels or the channel density must be increased. Either change will increase the efficiency of the biozone, since both changes result in more surface area across which mass transfer may occur. A channel spacing of 20 cm or a channel radius of 10 mm will result in a gas velocity of 3 cm/sec.

The mass transfer model developed in this work is very sensitive to the channel distribution. For instance, changing the average channel spacing from 1 m to 0.2 meter results in a TCE level in groundwater exiting the biozone of approximately 0.35 μg/l, which is below the MCL. The results of this calculation are included in Appendix A.

Reducing the channel spacing is or increasing the channel size beyond a certain value exposes a limitation of the mass balance approach used in this work. The model developed here assumes that the channels do not "communicate" with one another; the change in groundwater concentration due to mass flux from one channel does not affect the mass flux in or out of any other channel. When the channels are relatively widely spaced, biological activity will consume any compound entering the groundwater between the channels, and this is not a bad approximation. To account for this limitation, the aqueous concentration for a compound *j* was limited to the saturation concentration of the compound at the partial pressure appropriate for each channel element.

A second variable to which the model responds dramatically is the thickness of the stagnant water layer around each channel. If the layer thickness in the original calculation is increased to 1.0 mm, the TCE concentration in groundwater exiting the biozone rises to 63 μg/l. The results of this calculation are also included in Appendix A.

Table 3 summarizes the effect of several parameters on the bioremediation efficiency of the biozone. For the purposes of this table, efficiency represents the percentage of a compound's initial concentration removed as the plume passes through the biozone and is defined as

$$\varepsilon = 1 - \frac{C}{C_o} = 1 - e^{-k_{bio} t}$$

Seepage Velocity (m/day)	Stagnant Layer Thickness (mm)	Channel Spacing (m)	Channel Radius (mm)	k' (m^3/g-day)	ε %
(case study)					
2.7	*0.1*	*1.0*	*2.0*	*0.1*	56
1.0	*0.1*	*1.0*	*2.0*	*0.1*	89
2.7	**0.01**	*1.0*	*2.0*	*0.1*	99
2.7	**1.0**	*1.0*	*2.0*	*0.1*	9
2.7	*0.1*	**0.2**	*2.0*	*0.1*	99
2.7	*0.1*	*1.0*	**10**	*0.1*	98
2.7	*0.1*	*1.0*	*2.0*	**0.01**	8
2.7	*0.1*	*1.0*	*2.0*	**1.0**	99

Table 3 - Sensitivity Analysis

Italic text in Table 3 indicates values used in the original case study. Bold text highlights the parameter being varied to determine its effect on remediation efficiency. In general, it appears as though the biozone concept does offer some promise for stimulating bioremediation in large plumes. Only small deviations from the conservative assumptions used in the case study are necessary to obtain significant remediation efficiencies.

Because it takes into account the effects of pressure on gas concentration and the effects of porous media on diffusion, the channel element method is more realistic than the method presented by Johnson [1994] or Mohr [1995]. For the original case study parameters, their approach would have estimated a total oxygen flux of approximately 1.0×10^4 g/day versus the 1.4×10^5 g/day calculated here. Their estimate is low due to the increased flux at higher than atmospheric pressures and the increased thickness of the stagnant layer, although their use of an uncorrected diffusion coefficient does raise the value of their estimate to a small degree.

Chapter 7

Conclusions

7.1 Summary

When used primarily to deliver compounds necessary for bioremediation into solution, aquifer sparging is sometimes referred to as "biosparging." The purpose of this study is to investigate the feasibility of stimulating *in situ* bioremediation of large-scale groundwater contamination plumes via biosparging.

Many remediation experts believe that a network of unique gas channels forms when sparge gases are pumped into phreatic aquifers. Previous attempts to conceptually model mass transfer based on a channel network have sometimes failed to take into account variations in mass transfer arising from the physical features of natural aquifer systems. These features include the effects of greater than atmospheric pressures on gas solubility and the characteristics of diffusion in porous media.

A conceptual model employing small, representative sparge gas channel elements was developed to simulate the flow of gas in discrete channels and to investigate mass transfer mechanisms. Based on an assumed distribution of gas channels, average groundwater concentrations of various sparge gas compounds were calculated over the entire sparge zone. The groundwater concentrations were then used to estimate bioremediation rates for contaminated groundwater passing through the sparge zone.

The major conclusion of this work is that the biosparging appears to offer a viable method for stimulating bioremediation in large-scale groundwater

plumes. This conclusion was reached based on the use of conservative estimates of channel density, a diffusion-limited mass transfer process, and a realistic sparge gas mixture.

The factor most crucial to the success of the system is the spatial distribution and size of the sparge gas channels. This determines the width of the biozone and the reduced hydraulic conductivity due to sparging, which in turn determine the residence time of the plume in the biozone. The channel distribution and size also directly impacts the efficiency of mass transfer by increasing or decreasing the surface area of the gas/water interface. The effectiveness of the biozone also depends strongly on the average thickness of the stagnant boundary layer around each gas channel.

Additional conclusions include:

- Only channel spacing on the order of centimeters will result in significant reductions in hydraulic conductivity and associated plume deflection. Several field investigations have measured air saturations on the order of 40 percent in the area closest to a vertical sparge well, which implies channel spacing on the order of channel radii. For sparging operations at flow rates resulting in this magnitude of air saturation, the zone close to and above the sparge point may resemble the unsaturated conditions normally associated with the vadose zone. At the same time, sparge gas may flow in distinct channels at greater radial distances from the sparge point.

- The use of effective diffusion coefficients is necessary to prevent overestimating the efficiency of sparging mass transfer.

- Pressure effects must be taken into account to prevent underestimating the efficiency of sparging mass transfer.

- Sparge gas channel diameters or vertical gas velocities will tend to increase as the gas flows upward from the sparge point. There is some

evidence that gas in channels located a significant distance from the sparging injection point will flow at a constant velocity.

- Sparge gas injected via a vertical well will most likely flow from the top of the well screen.

7.2 Future Research

This work is largely based on the premise that discrete gas channels form as a result of sparging, a premise that has never been proven in three dimensions. The biggest challenge for future research is to develop a better understanding of the actual gas flow regime in heterogeneous porous media.

One possible method to accurately indicate the three-dimensional flow of sparge gases in the lab was briefly investigated as part of this study. The proposed procedure requires a lab-scale "sandbox" filled with a very light-colored saturated sand of any grain size distribution. The "groundwater" is spiked with a dilute solution of manganese sulfate, which is colorless at low concentrations and very stable. Ozone is injected to simulate a sparge gas, and as it travels up through the saturated sand it oxidized the manganese, causing it to precipitate. The precipitate is very dark brown and will quickly be attracted to any nearby sand grains, effectively "staining" the flowpath of the ozone. The reaction occurs on the order of seconds and the ozone will not diffuse appreciable away from the flow channel. The flowpaths must then be reconstructed by draining the sandbox and manually excavating the sand to create a series of horizontal cross sections. Only the ozone / manganese sulfate reaction portion of this procedure was tested; no sandbox was constructed. Nonetheless, the procedure may offer a relatively inexpensive (albeit painstaking) method to investigate sparge gas flow in three dimensions.

The biozone was treated as a lumped bioreactor in this work. If gas channels do form, they will act more as individual point sources for small scale bioreactors, and bioremediation will occur in a "streaky" fashion downgradient of the channels throughout the biozone. A more detailed modeling of the

biotransformation process, including the effects of vertical stratification, would provide further insight into the biosparging process.

Numerous parameters crucial to the success of the biozone, such as seepage velocity and microbiological constants, were only known within a range and had to be estimated. Conservative estimates were consistently made; more precise knowledge of such parameters would provide a better measure of the feasibility of the biozone concept.

Finally, the utility of the model developed here is based on the assumption that the mass transfer into and out of each gas channel is independent of all other channels. A further refinement would include a coupled system of equations describing both the mass transfer in and out of the gas channels and in and out of the groundwater due to consumption by microorganisms, mass transfer to and from gas channels, or sorption. This refinement will be particularly important in the case of high channel density and/or large channels because the current model will overestimate mass transfer from the gas channels to the water in such circumstances.

References

Acomb, L. J., D. McKay, P. Currier, S. T. Berglund, T. V. Sherhart, and C. V. Benediktsson, Neutron Probe Measurements of Air Saturation Near an Air Sparging Well, in *In Situ Aeration: Air Sparging, Bioventing, and Related Remediation Processes*, edited by R. E. Hinchee, R. N. Miller, and P. C. Johnson, pp. 47-61, Batelle Press, Columbus, OH, 1995.

Advanced Sciences, Inc., *Final Design Package for the F2-12 Product Recovery System*, Massachusetts Military Reservation, 1995.

Ahlfield, D. P., A. Dahmani, W. Ji., A Conceptual Model of Field Behavior of Air Sparging and its Implications for Application, *Ground Water Monitoring and Review, Fall 1994*, 132-139, 1994.

American Petroleum Institute (API), *In Situ Air Sparging: Evaluation of Petroleum Industry Sites and Considerations for Applicability, Design and Operation*, API Publication Number 4609, API, Washington, D.C., 1995.

Bear, J., *Dynamics of Fluids in Porous Media*, Dover Publications, Inc., New York, NY, 1972.

Bedient, P. B., H. S. Rifai, and C. J. Newell, *Ground Water Contamination: Transport and Remediation*, Prentice-Hall, Inc., 1994.

Binning, P., M. A. Celia, J. C. Johnson, *Auxiliary Analyses in Support of Performance Assessment of a Hypothetical Low-Level Waste Facility*, U. S. Nuclear Regulatory Commission Publication NUREG/CR-6114, Washington, D.C., 1995.

Boersma, P. M., K. R. Piontek, and P. A. B. Newman, Sparging Effectiveness for Groundwater Restoration, in *In Situ Aeration: Air Sparging, Bioventing, and Related Remediation Processes*, edited by R. E. Hinchee, R. N. Miller, and P. C. Johnson, pp. 39-46, Batelle Press, Columbus, OH, 1995.

CDM Federal Programs Corporation, *Remedial Investigation, Main Base Landfill (AOC LF-1) and Hydrogeologic Region I Study*, Massachusetts Military Reservation, 1995.

Clayton, W. S., R. A. Brown, and D. H. Bass, Air Sparging and Bioremediation: The Case for In Situ Mixing, in *In Situ Aeration: Air Sparging, Bioventing, and Related Remediation Processes*, edited by R. E. Hinchee, R. N. Miller, and P. C. Johnson, pp. 75-85, Batelle Press, Columbus, OH, 1995.

Cooke, J. R., D. C. Davis, and E. T. Sobel, *MacPoisson™*, Cooke Publications, Ithaca, NY, 1989.

Dullien, F. A. L., *Porous Media, Fluid Transport and Pore Structure*, Academic Press, NY, 1979.

Eddy, C. A., B. B. Looney, J. M. Dougherty, T. C. Hazen, and D. S. Kaback, *Characterization of the Geology, Geochemistry, Hydrology, and Microbiology of the In-Situ Air Stripping Demonstration Site at the Savannah River Site*, Document WSRC-RD-91-21, 1991.

Greenkorn, R. A., *Flow Phenomena in Porous Media*, Marcel Dekker, Inc., New York, NY, 1983.

Hazen, Terry C., *Preliminary Technology Report for In-Situ Bioremediation Demonstration (Methane Biostimulation) of the Savannah River Integrated Demonstration Project, DOE/OTD*, Document WSRC-TR-93-670, Rev. 0, 1995.

Henry, S. M. and D. Grbic-Galic, Biodegradation of Trichloroethylene in Methanotrophic Systems and Implications for Process Applications, in *Biological Degradation and Bioremediation of Toxic Chemicals*, edited by G. R. Chaudhry, pp. 314-344, Chapman and Hall, London, 1994.

Hinchee, R. E. (Ed.), *Air Sparging for Site Remediation*, CRC Press, Boca Raton, Fl, 1994a.

Hinchee, R. E., Air Sparging State of the Art, in *Air Sparging for Site Remediation*, edited by R. E. Hinchee, CRC Press, Boca Raton, Fl, 1994b.

Hinchee, R. E., R. N. Miller, and P. C. Johnson (Eds.), *In Situ Aeration: Air Sparging, Bioventing, and Related Remediation Processes*, Batelle Press, Columbus, OH, 1995.

Johnson, R. L., Enhancing Biodegradation with In Situ Air Sparging: A Conceptual Model, in *Air Sparging for Site Remediation*, edited by R. E. Hinchee, pp. 14-21, CRC Press, Boca Raton, Fla., 1994.

Johnson, R. L., P. C. Johnson, D. B. McWhorter, R. E. Hinchee, and I Goodman, An Overview of In Situ Air Sparging, Groundwater *Monitoring and Review, Fall 1993*, 127-135, 1993.

Leeson, A, R. E. Hinchee, G. L. Headington, and C. M. Vogel, Air Channel Distribution During Air Sparging: A Field Experiment, in *In Situ Aeration: Air Sparging, Bioventing, and Related Remediation Processes*, edited by R. E. Hinchee, R. N. Miller, and P. C. Johnson, pp. 215-222, Batelle Press, Columbus, OH, 1995.

Lide, D. R., and H. P. R. Frederikse, *CRC Handbook of Chemistry and Physics*, CRC Press, Boca Raton, FL, 1993

Lundegard, P. D., Air Sparging: Much Ado About Mounding, in *In Situ Aeration: Air Sparging, Bioventing, and Related Remediation Processes*, edited by R. E. Hinchee, R. N. Miller, and P. C. Johnson, pp. 21-29, Batelle Press, Columbus, OH, 1995.

Lundegard, P., Actual Versus Apparent Radius of Influence: An Air Sparging Pilot Test in a Sandy Aquifer, in *Proceedings of the 1994 Petroleum Hydrocarbon and Organic Chemicals in Groundwater Prevention, Detection, and Restoration Conference*, pp. 191-206, Houston, TX, 1994.

McWhorter, D. B. and D. K. Sunada, Exact Integral Solutions for Two-Phase Flow, *Water Resources Research, 26*(3), 81-92, 1989.

Mohr, D. H., Mass Transfer Concepts Applied to In Situ Air Sparging, paper delivered at *The Third International Symposium on In Situ and On-Site Bioreclamation*, April 24-27, 1995, San Diego, CA, 1995.

Mohtar, R. H., R. B. Wallace, and L. J. Segerlind, Finite Element Simulation of Oil Spill Cleanup Using Air Sparging, in *Computational Methods in Water Resources X*, edited by A. Peters, pp. 967-974, Kluwer Academic Publishers, the Netherlands, 1994.

National Research Council, *In Situ Bioremediation: When does it work?*, National Academy Press, Washington, D. C., 1993.

Plummer, C. R., A Laboratory Study of Well Configurations of *In Situ* Air Sparging, M.S. Thesis, 206 pp., College of Engineering, Louisiana Tech University, 1994.

Schwarzenbach, R. P., P. M. Gschwend, and D. M Imboden, *Environmental Organic Chemistry*, John Wiley & Sons, New York, NY, 1993.

Semprini, L., G. D. Hopkins, P. V. Roberts, and P. L. McCarty, Pilot Scale Field Studies of in situ bioremediation of chlorinated solvents, *Journal of Hazardous Materials, 32*, 145-162, 1990.

Semprini, L., P. V. Roberts, G. D. Hopkins, and P. L. McCarty, A Field Evaluation of In-Situ Biodegradation of Chlorinated Ethenes: Part 2, Results of Biostimulation and Biotransformation Experiments, *Ground Water, 28*(5), 715-727, 1990.

Sleep, B. E., and J. F. Sykes, Modeling the Transport of Volatile Organics in Variably Saturated Media, *Water Resources Research, 25*(1), 399-413, 1990.

U. S. Department of Energy, Office of Environmental Management, *In Situ Bioremediation Using Horizontal Wells, Innovative Technology Summary Report*, 1995.

van Dijke, M. I. J. and S. E. A. T. M. van der Zee, Multi-Phase Flow Modeling of Air Injection in Ground Water, in *Computational Methods in Water Resources X*, edited by A. Peters, pp. 933-940, Kluwer Academic Publishers, the Netherlands, 1994.

Wackett, L. P., Bacterial Co-Metabolism of Halogenated Organic Compounds, in *Microbial Transformation and Degradation of Toxic Organic Chemicals*, edited by L. Y. Young and C. E. Cerniglia, pp. 217-241, Wiley-Liss, Inc., New York, NY, 1995.

Wei, J., A. Dahmani, D. P. Ahlfeld, J. D. Lin, and E. Hill, Laboratory Study of Air Sparging: Air Flow Visualization, *Groundwater Monitoring and Review, Fall 1993*, 115-126, 1993.

Wilson, D. J., S. Kayano, R. D. Mutch, Jr., and A. N. Clarke, Groundwater Cleanup by in-situ Sparging. I. Mathematical Modeling, *Separation Science and Technology, (27)*, 1023-1041, 1992.

Appendix A

Channel Element Analyses

Three sets of channel analyses are included in this Appendix. For each set, the first page lists the pertinent physical constants and parameters necessary for mass balance calculations, as well as the biozone efficiency and significant results of the analysis for oxygen, methane, TCE, and PCE. The next five pages of each set show the calculations on an channel element-by-element basis for each of the compounds in the system.

INPUT DATA - ORIGINAL CASE STUDY						CALCULATED CONSTANTS (at T °C)	RESULTS	
Groundwater Temperature ("T" °C)	Aquifer Porosity (decimal)	Seepage Velocity (m/day)	Min. Entry Pressure (m water)	Tortuosity Factor	l_t (mm)	# Channels 120,000	Total Oxygen Delivery (g/day)	Total Methane Delivery (g/day)
10	0.25	2.7	0.20	0.6	0.1		2.33E+05	1.73E+04
Inject. Rate (ft^3/min)	Inject. Rate (m^3/sec)	Biozone Width (m)	Channel Interval (m)	Channel Radius (mm)	Well Length (m)	Flow / Channel (m^3/sec)	Average Oxygen Concentration (g/m3)	Average Methane Concentration (g/m3)
600	0.2834	60	1	2	2000	2.36E-06	6.24	0.46
COMPOUND	m^1 (g/mol)	K_h @ T °C	D_w @ T °C (cm^3/sec)	x^1 in sparge gas (decimal)	C_o in groundwater (g/m^3)	$D_{w,eff}$ (cm^3/sec)	PCE Flux to Vadose Zone (g/sec-m^2)	TCE Flux to Vadose Zone (g/sec-m^2)
Oxygen	32	25.6	1.50E-05	0.19	0.00	2.25E-06	2.21E-08	2.19E-08
Nitrogen	28	52.3	1.21E-05	0.77	0.00	1.82E-06		
Methane	16	23.3	9.62E-06	0.04	0.00	1.44E-06	k' (m^3/g-day) 0.1	k bio (1/day) 0.037
PCE	165.8	0.31	6.10E-06	0.00	0.07	9.15E-07		
TCE	131.4	0.17	6.75E-06	0.00	0.07	1.01E-06	EFFICIENCY: 0.56084	

Oxygen

Channel Element #	Depth (m)	mol fraction	Cg (g/m3)	C^g (g/m3)	Qj Into Bottom of Channel Element (m3/sec)	Mass Flux Across Wall (g/sec)	Mass Flux Into Bottom of Channel Element (g/sec)
0	Vadose Zone						2.42E-03
1	0-1	0.1892	291.18	11.37		3.30E-07	2.42E-03
2	1-2	0.1892	316.74	12.37		3.58E-07	2.43E-03
3	2-3	0.1892	342.30	13.37		3.87E-07	2.43E-03
4	3-4	0.1892	367.86	14.37		4.16E-07	2.43E-03
5	4-5	0.1892	393.44	15.37		4.45E-07	2.43E-03
6	5-6	0.1893	419.02	16.37		4.74E-07	2.43E-03
7	6-7	0.1893	444.61	17.37		5.03E-07	2.43E-03
8	7-8	0.1893	470.20	18.37		5.32E-07	2.43E-03
9	8-9	0.1893	495.81	19.37		5.61E-07	2.43E-03
10	9-10	0.1893	521.42	20.37		5.90E-07	2.43E-03
11	10-11	0.1894	547.04	21.37		6.19E-07	2.43E-03
12	11-12	0.1894	572.67	22.37		6.48E-07	2.43E-03
13	12-13	0.1894	598.31	23.37		6.77E-07	2.43E-03
14	13-14	0.1894	623.96	24.37		7.06E-07	2.43E-03
15	14-15	0.1895	649.62	25.38		7.35E-07	2.43E-03
16	15-16	0.1895	675.30	26.38		7.64E-07	2.43E-03
17	16-17	0.1895	700.98	27.38		7.93E-07	2.43E-03
18	17-18	0.1895	726.68	28.39		8.22E-07	2.43E-03
19	18-19	0.1896	752.39	29.39		8.52E-07	2.44E-03
20	19-20	0.1896	778.11	30.39		8.81E-07	2.44E-03
21	20-21	0.1896	803.84	31.40		9.10E-07	2.44E-03
22	21-22	0.1897	829.59	32.41		9.39E-07	2.44E-03
23	22-23	0.1897	855.36	33.41		9.68E-07	2.44E-03
24	23-24	0.1898	881.14	34.42		9.97E-07	2.44E-03
25	24-25	0.1898	906.93	35.43		1.03E-06	2.44E-03
26	25-26	0.1898	932.74	36.44		1.06E-06	2.44E-03
27	26-27	0.1899	958.56	37.44		1.08E-06	2.44E-03
28	27-28	0.1899	984.41	38.45		1.11E-06	2.44E-03
29	28-29	0.1900	1010.26	39.46		1.14E-06	2.45E-03
30	29-30	0.1900	1036.14	40.47	2.36E-06	1.17E-06	2.45E-03
	Maximum Average Oxygen Concentration =			**25.89**		**2.25E-05**	**= Total Oxygen Flux Per Channel**

Nitrogen

Channel Element #	Depth (m)	mol fraction	Cg (g/m3)	C^g (g/m3)	Qj into Bottom of Channel Element (m3/sec)	Mass Flux Across Wall (g/sec)	Mass Flux into Bottom of Channel Element (g/sec)
0	Vadose Zone						8.65E-03
1	0-1	0.7709	1038.25	19.85		4.64E-07	8.65E-03
2	1-2	0.7709	1129.27	21.59		5.05E-07	8.65E-03
3	2-3	0.7709	1220.28	23.33		5.46E-07	8.65E-03
4	3-4	0.7708	1311.29	25.07		5.87E-07	8.65E-03
5	4-5	0.7708	1402.30	26.81		6 27E-07	8.65E-03
6	5-6	0.7708	1493.29	28.55		6.68E-07	8.65E-03
7	6-7	0.7708	1584.28	30.29		7.09E-07	8.65E-03
8	7-8	0.7708	1675.27	32.03		7.49E-07	8.65E-03
9	8-9	0.7707	1766.24	33.77		7.90E-07	8.65E-03
10	9-10	0.7707	1857.21	35.51		8.31E-07	8.65E-03
11	10-11	0.7707	1948.17	37.25		8.71E-07	8.65E-03
12	11-12	0.7707	2039.12	38.99		9.12E-07	8.65E-03
13	12-13	0.7706	2130.06	40.73		9.53E-07	8.65E-03
14	13-14	0.7706	2220.99	42.47		9.93E-07	8.66E-03
15	14-15	0.7706	2311.91	44.20		1.03E-06	8.66E-03
16	15-16	0.7706	2402.82	45.94		1.07E-06	8.66E-03
17	16-17	0.7705	2493.71	47.68		1.12E-06	8.66E-03
18	17-18	0.7705	2584.60	49.42		1.16E-06	8.66E-03
19	18-19	0.7705	2675.48	51.16		1.20E-06	8.66E-03
20	19-20	0.7704	2766.34	52.89		1.24E-06	8.66E-03
21	20-21	0.7704	2857.19	54.63		1.28E-06	8.66E-03
22	21-22	0.7703	2948.03	56.37		1.32E-06	8.66E-03
23	22-23	0.7703	3038.85	58.10		1.36E-06	8.67E-03
24	23-24	0.7703	3129.66	59.84		1.40E-06	8.67E-03
25	24-25	0.7702	3220.46	61.58		1.44E-06	8.67E-03
26	25-26	0.7702	3311.24	63.31		1.48E-06	8.67E-03
27	26-27	0.7701	3402.00	65.05		1.52E-06	8.67E-03
28	27-28	0.7701	3492.75	66.78		1.56E-06	8.67E-03
29	28-29	0.7700	3583.49	68.52		1.60E-06	8.68E-03
30	29-30	0.7700	3674.21	70.25	2.36E-06	1.64E-06	8.68E-03

Methane

Channel Element #	Depth (m)	mol fraction	Cg (g/m3)	C^g (g/m3)	Qj into Bottom of Channel Element (m^3/sec)	Mass Flux Across Wall (g/sec)	Mass Flux Into Bottom of Channel Element (g/sec)
0	Vadose Zone						2.56E-04
1	0-1	3.99E-02	30.7333	1.3190		2.45E-08	2.56E-04
2	1-2	3.99E-02	33.4292	1.4347		2.66E-08	2.56E-04
3	2-3	3.99E-02	36.1252	1.5504		2.88E-08	2.56E-04
4	3-4	3.99E-02	38.8215	1.6662		3.09E-08	2.56E-04
5	4-5	3.99E-02	41.5181	1.7819		3.31E-08	2.56E-04
6	5-6	3.99E-02	44.2150	1.8976		3.52E-08	2.56E-04
7	6-7	3.99E-02	46.9121	2.0134		3.74E-08	2.56E-04
8	7-8	3.99E-02	49.6095	2.1292		3.95E-08	2.56E-04
9	8-9	3.99E-02	52.3073	2.2449		4.17E-08	2.56E-04
10	9-10	3.99E-02	55.0054	2.3607		4.38E-08	2.56E-04
11	10-11	3.99E-02	57.7039	2.4766		4.60E-08	2.56E-04
12	11-12	4.00E-02	60.4028	2.5924		4.81E-08	2.56E-04
13	12-13	4.00E-02	63.1021	2.7082		5.03E-08	2.56E-04
14	13-14	4.00E-02	65.8017	2.8241		5.25E-08	2.56E-04
15	14-15	4.00E-02	68.5019	2.9400		5.46E-08	2.56E-04
16	15-16	4.00E-02	71.2024	3.0559		5.68E-08	2.57E-04
17	16-17	4.00E-02	73.9035	3.1718		5.89E-08	2.57E-04
18	17-18	4.00E-02	76.6050	3.2878		6.11E-08	2.57E-04
19	18-19	4.00E-02	79.3070	3.4037		6.32E-08	2.57E-04
20	19-20	4.00E-02	82.0095	3.5197		6.54E-08	2.57E-04
21	20-21	4.00E-02	84.7126	3.6357		6.75E-08	2.57E-04
22	21-22	4.00E-02	87.4163	3.7518		6.97E-08	2.57E-04
23	22-23	4.00E-02	90.1205	3.8678		7.18E-08	2.57E-04
24	23-24	4.00E-02	92.8253	3.9839		7.40E-08	2.57E-04
25	24-25	4.00E-02	95.5307	4.1000		7.62E-08	2.57E-04
26	25-26	4.00E-02	98.2367	4.2162		7.83E-08	2.57E-04
27	26-27	4.00E-02	100.9433	4.3323		8.05E-08	2.57E-04
28	27-28	4.00E-02	103.6507	4.4485		8.26E-08	2.57E-04
29	28-29	4.00E-02	106.3587	4.5647		8.48E-08	2.57E-04
30	29-30	4.00E-02	109.0674	4.6810	2.36E-06	8.69E-08	2.58E-04
	Maximum Average Methane Concentration =			2.9987		1.67E-06	= Total Methane Flux Per Channel

PCE

Channel Element #	Depth (m)	mol fraction	Cg (g/m3)	C^g (g/m3)	Qj into Bottom of Channel Element (m^3/sec)	Mass Flux Across Wall (g/sec)	Mass Flux into Bottom of Channel Element (g/sec)	
0	Vadose Zone						2.21E-08	= Per Channel Flux of
1	0-1	3.21E-07	0.0026	0.0081		-7.29E-10	2.13E-08	PCE into Vadose Zone
2	1-2	3.10E-07	0.0027	0.0085		-7.24E-10	2.06E-08	
3	2-3	2.99E-07	0.0028	0.0089		-7.20E-10	1.99E-08	
4	3-4	2.88E-07	0.0029	0.0092		-7.16E-10	1.92E-08	
5	4-5	2.78E-07	0.0030	0.0095		-7.13E-10	1.85E-08	
6	5-6	2.67E-07	0.0031	0.0097		-7.10E-10	1.77E-08	
7	6-7	2.56E-07	0.0031	0.0099		-7.08E-10	1.70E-08	
8	7-8	2.46E-07	0.0032	0.0100		-7.06E-10	1.63E-08	
9	8-9	2.35E-07	0.0032	0.0101		-7.05E-10	1.56E-08	
10	9-10	2.24E-07	0.0032	0.0102		-7.05E-10	1.49E-08	
11	10-11	2.14E-07	0.0032	0.0102		-7.05E-10	1.42E-08	
12	11-12	2.03E-07	0.0032	0.0101		-7.06E-10	1.35E-08	
13	12-13	1.92E-07	0.0032	0.0100		-7.07E-10	1.28E-08	
14	13-14	1.82E-07	0.0031	0.0099		-7.09E-10	1.21E-08	
15	14-15	1.71E-07	0.0030	0.0097		-7.11E-10	1.14E-08	
16	15-16	1.60E-07	0.0030	0.0094		-7.14E-10	1.07E-08	
17	16-17	1.49E-07	0.0029	0.0091		-7.17E-10	9.95E-09	
18	17-18	1.39E-07	0.0028	0.0087		-7.22E-10	9.23E-09	
19	18-19	1.28E-07	0.0026	0.0083		-7.26E-10	8.50E-09	
20	19-20	1.17E-07	0.0025	0.0079		-7.32E-10	7.77E-09	
21	20-21	1.06E-07	0.0023	0.0074		-7.38E-10	7.03E-09	
22	21-22	9.44E-08	0.0021	0.0068		-7.45E-10	6.29E-09	
23	22-23	8.31E-08	0.0019	0.0062		-7.52E-10	5.53E-09	
24	23-24	7.16E-08	0.0017	0.0055		-7.60E-10	4.77E-09	
25	24-25	6.01E-08	0.0015	0.0047		-7.69E-10	4.00E-09	
26	25-26	4.84E-08	0.0012	0.0039		-7.79E-10	3.23E-09	
27	26-27	3.65E-08	0.0010	0.0030		-7.89E-10	2.44E-09	
28	27-28	2.45E-08	0.0007	0.0021		-8.00E-10	1.64E-09	
29	28-29	1.24E-08	0.0003	0.0011		-8.12E-10	8.25E-10	
30	29-30	0.00E+00	0.0000	0.0000	2.36E-06	-8.25E-10	0	

TCE

Channel Element #	Depth (m)	mol fraction	Cg (g/m3)	C^g (g/m3)	Qj into Bottom of Channel Element (m3/sec)	Mass Flux Across Wall (g/sec)	Mass Flux into Bottom of Channel Element (g/sec)	
0	Vadose Zone						2.19E-08	= Per Channel Flux of
1	0-1	4.02E-07	0.0025	0.0146		-7.22E-10	2.12E-08	TCE Into Vadose Zone
2	1-2	3.89E-07	0.0027	0.0154		-7.12E-10	2.05E-08	
3	2-3	3.75E-07	0.0028	0.0160		-7.04E-10	1.97E-08	
4	3-4	3.62E-07	0.0029	0.0166		-6.96E-10	1.91E-08	
5	4-5	3.49E-07	0.0030	0.0171		-6.89E-10	1.84E-08	
6	5-6	3.36E-07	0.0031	0.0175		-6.84E-10	1.77E-08	
7	6-7	3.23E-07	0.0031	0.0179		-6.79E-10	1.70E-08	
8	7-8	3.10E-07	0.0032	0.0182		-6.76E-10	1.63E-08	
9	8-9	2.97E-07	0.0032	0.0184		-6.73E-10	1.56E-08	
10	9-10	2.84E-07	0.0032	0.0185		-6.72E-10	1.50E-08	
11	10-11	2.72E-07	0.0032	0.0185		-6.71E-10	1.43E-08	
12	11-12	2.59E-07	0.0032	0.0185		-6.72E-10	1.36E-08	
13	12-13	2.46E-07	0.0032	0.0183		-6.73E-10	1.30E-08	
14	13-14	2.33E-07	0.0032	0.0181		-6.76E-10	1.23E-08	
15	14-15	2.20E-07	0.0031	0.0178		-6.80E-10	1.16E-08	
16	15-16	2.07E-07	0.0030	0.0174		-6.85E-10	1.09E-08	
17	16-17	1.94E-07	0.0029	0.0169		-6.92E-10	1.02E-08	
18	17-18	1.81E-07	0.0028	0.0163		-6.99E-10	9.53E-09	
19	18-19	1.67E-07	0.0027	0.0157		-7.08E-10	8.82E-09	
20	19-20	1.54E-07	0.0026	0.0149		-7.19E-10	8.10E-09	
21	20-21	1.40E-07	0.0024	0.0140		-7.30E-10	7.37E-09	
22	21-22	1.26E-07	0.0023	0.0130		-7.44E-10	6.63E-09	
23	22-23	1.11E-07	0.0021	0.0118		-7.58E-10	5.87E-09	
24	23-24	9.65E-08	0.0018	0.0106		-7.75E-10	5.09E-09	
25	24-25	8.14E-08	0.0016	0.0092		-7.93E-10	4.30E-09	
26	25-26	6.60E-08	0.0013	0.0077		-8.13E-10	3.49E-09	
27	26-27	5.02E-08	0.0010	0.0060		-8.34E-10	2.65E-09	
28	27-28	3.40E-08	0.0007	0.0042		-8.58E-10	1.80E-09	
29	28-29	1.73E-08	0.0004	0.0022		-8.84E-10	9.12E-10	
30	29-30	0.00	0.0000	0.0000	2.36E-06	-9.12E-10	0.00E+00	

INPUT DATA - HORIZONTAL SPARGE WELL						CALCULATED CONSTANTS (at T °C)	RESULTS	
Groundwater Temperature ("T" °C)	Aquifer Porosity (decimal)	Seepage Velocity (m/day)	Min. Entry Pressure (m water)	Tortuosity Factor	l_t (mm)	# Channels 3,000,000	Total Oxygen Delivery (g/day)	Total Methane Delivery (g/day)
10	0.25	2.7	0.20	0.6	0.1		5.53E+06	4.24E+05
Inject. Rate (ft^3/min)	Inject. Rate (m^3/sec)	Biozone Width (m)	Channel Interval (m)	Channel Radius (mm)	Well Length (m)	Flow / Channel (m^3/sec)	Average Oxygen Concentration (g/m3)	Average Methane Concentration (g/m3)
600	0.2834	60	0.2	2	2000	9.45E-08	24.55	2.94
COMPOUND	m^1 (g/mol)	K_h @ T °C	D_w @ T °C (cm^3/sec)	x^1 in sparge gas (decimal)	C_o in groundwater (g/m^3)	$D_{w\,eff}$ (cm^3/sec)	PCE Flux to Vadose Zone ($g/sec-m^2$)	TCE Flux to Vadose Zone ($g/sec-m^2$)
Oxygen	32	25.6	1.50E-05	0.19	0.00	2.25E-06	4.88E-09	3.07E-09
Nitrogen	28	52.3	1.21E-05	0.77	0.00	1.82E-06		
Methane	16	23.3	9.62E-06	0.04	0.00	1.44E-06	k' (m^3/g-day) 0.1	k bio (1/day) 0.235
PCE	165.8	0.31	6.10E-06	0.00	0.07	9.15E-07		
TCE	131.4	0.17	6.75E-06	0.00	0.07	1.01E-06	EFFICIENCY: 0.99460	

Oxygen

Channel Element #	Depth (m)	mol fraction	Cg (g/m3)	C^g (g/m3)	Qj into Bottom of Channel Element (m3/sec)	Mass Flux Across Wall (g/sec)	Mass Flux into Bottom of Channel Element (g/sec)
0	Vadose Zone						7.65E-05
1	0-1	0.1689	260.04	10.16		2.94E-07	7.68E-05
2	1-2	0.1693	283.42	11.07		3.21E-07	7.71E-05
3	2-3	0.1697	306.95	11.99		3.47E-07	7.75E-05
4	3-4	0.1701	330.63	12.92		3.74E-07	7.79E-05
5	4-5	0.1705	354.47	13.85		4.01E-07	7.83E-05
6	5-6	0.1709	378.49	14.78		4.28E-07	7.87E-05
7	6-7	0.1714	402.71	15.73		4.56E-07	7.92E-05
8	7-8	0.1719	427.12	16.68		4.83E-07	7.96E-05
9	8-9	0.1725	451.74	17.65		5.11E-07	8.02E-05
10	9-10	0.1731	476.58	18.62		5.39E-07	8.07E-05
11	10-11	0.1736	501.65	19.60		5.68E-07	8.13E-05
12	11-12	0.1743	526.97	20.58		5.96E-07	8.19E-05
13	12-13	0.1749	552.54	21.58		6.25E-07	8.25E-05
14	13-14	0.1756	578.37	22.59		6.55E-07	8.31E-05
15	14-15	0.1763	604.48	23.61		6.84E-07	8.38E-05
16	15-16	0.1770	630.87	24.64		7.14E-07	8.45E-05
17	16-17	0.1778	657.56	25.69		7.44E-07	8.53E-05
18	17-18	0.1786	684.56	26.74		7.75E-07	8.61E-05
19	18-19	0.1794	711.87	27.81		8.06E-07	8.69E-05
20	19-20	0.1802	739.51	28.89		8.37E-07	8.77E-05
21	20-21	0.1811	767.49	29.98		8.69E-07	8.86E-05
22	21-22	0.1820	795.82	31.09		9.01E-07	8.95E-05
23	22-23	0.1829	824.50	32.21		9.33E-07	9.04E-05
24	23-24	0.1838	853.56	33.34		9.66E-07	9.14E-05
25	24-25	0.1848	882.99	34.49		9.99E-07	9.24E-05
26	25-26	0.1858	912.80	35.66		1.03E-06	9.34E-05
27	26-27	0.1868	943.02	36.84		1.07E-06	9.45E-05
28	27-28	0.1878	973.64	38.03		1.10E-06	9.56E-05
29	28-29	0.1889	1004.68	39.25		1.14E-06	9.67E-05
30	29-30	0.1900	1036.14	40.47	9.45E-08	1.17E-06	9.79E-05
	Maximum Average Oxygen Concentration =			24.55		2.13E-05	= Total Oxygen Flux Per Channel

Nitrogen

Channel Element #	Depth (m)	mol fraction	Cg (g/m3)	C^g (g/m3)	Qj into Bottom of Channel Element (m3/sec)	Mass Flux Across Wall (g/sec)	Mass Flux into Bottom of Channel Element (g/sec)
0	Vadose Zone						3.15E-04
1	0-1	0.7928	1067.81	20.42		4.78E-07	3.15E-04
2	1-2	0.7925	1160.89	22.20		5.19E-07	3.16E-04
3	2-3	0.7921	1253.83	23.97		5.61E-07	3.17E-04
4	3-4	0.7916	1346.63	25.75		6.02E-07	3.17E-04
5	4-5	0.7912	1439.27	27.52		6.44E-07	3.18E-04
6	5-6	0.7907	1531.74	29.29		6.85E-07	3.18E-04
7	6-7	0.7901	1624.03	31.05		7.26E-07	3.19E-04
8	7-8	0.7896	1716.14	32.81		7.68E-07	3.20E-04
9	8-9	0.7890	1808.04	34.57		8.09E-07	3.21E-04
10	9-10	0.7884	1899.73	36.32		8.50E-07	3.22E-04
11	10-11	0.7877	1991.20	38.07		8.91E-07	3.23E-04
12	11-12	0.7870	2082.45	39.82		9.31E-07	3.23E-04
13	12-13	0.7863	2173.45	41.56		9.72E-07	3.24E-04
14	13-14	0.7856	2264.20	43.29		1.01E-06	3.25E-04
15	14-15	0.7848	2354.69	45.02		1.05E-06	3.27E-04
16	15-16	0.7840	2444.91	46.75		1.09E-06	3.28E-04
17	16-17	0.7832	2534.84	48.47		1.13E-06	3.29E-04
18	17-18	0.7824	2624.49	50.18		1.17E-06	3.30E-04
19	18-19	0.7815	2713.84	51.89		1.21E-06	3.31E-04
20	19-20	0.7806	2802.88	53.59		1.25E-06	3.32E-04
21	20-21	0.7797	2891.60	55.29		1.29E-06	3.34E-04
22	21-22	0.7787	2979.99	56.98		1.33E-06	3.35E-04
23	22-23	0.7777	3068.04	58.66		1.37E-06	3.36E-04
24	23-24	0.7767	3155.75	60.34		1.41E-06	3.38E-04
25	24-25	0.7756	3243.10	62.01		1.45E-06	3.39E-04
26	25-26	0.7746	3330.09	63.67		1.49E-06	3.41E-04
27	26-27	0.7735	3416.70	65.33		1.53E-06	3.42E-04
28	27-28	0.7723	3502.93	66.98		1.57E-06	3.44E-04
29	28-29	0.7712	3588.77	68.62		1.61E-06	3.45E-04
30	29-30	0.7700	3674.21	70.25	9.45E-08	1.64E-06	3.47E-04

Methane

Channel Element #	Depth (m)	mol fraction	Cg (g/m3)	C^g (g/m3)	Qj into Bottom of Channel Element (m^3/sec)	Mass Flux Across Wall (g/sec)	Mass Flux Into Bottom of Channel Element (g/sec)
0	Vadose Zone						8.67E-06
1	0-1	3.82E-02	29.4109	1.2623		2.34E-08	8.69E-06
2	1-2	3.82E-02	32.0159	1.3741		2.55E-08	8.72E-06
3	2-3	3.83E-02	34.6272	1.4861		2.76E-08	8.74E-06
4	3-4	3.83E-02	37.2455	1.5985		2.97E-08	8.77E-06
5	4-5	3.84E-02	39.8710	1.7112		3.18E-08	8.80E-06
6	5-6	3.84E-02	42.5043	1.8242		3.39E-08	8.84E-06
7	6-7	3.84E-02	45.1459	1.9376		3.60E-08	8.87E-06
8	7-8	3.85E-02	47.7961	2.0513		3.81E-08	8.91E-06
9	8-9	3.85E-02	50.4554	2.1655		4.02E-08	8.95E-06
10	9-10	3.86E-02	53.1242	2.2800		4.23E-08	8.99E-06
11	10-11	3.86E-02	55.8030	2.3950		4.45E-08	9.04E-06
12	11-12	3.87E-02	58.4922	2.5104		4.66E-08	9.09E-06
13	12-13	3.87E-02	61.1921	2.6263		4.88E-08	9.13E-06
14	13-14	3.88E-02	63.9031	2.7426		5.09E-08	9.19E-06
15	14-15	3.89E-02	66.6257	2.8595		5.31E-08	9.24E-06
16	15-16	3.89E-02	69.3602	2.9768		5.53E-08	9.29E-06
17	16-17	3.90E-02	72.1068	3.0947		5.75E-08	9.35E-06
18	17-18	3.91E-02	74.8661	3.2131		5.97E-08	9.41E-06
19	18-19	3.91E-02	77.6383	3.3321		6.19E-08	9.47E-06
20	19-20	3.92E-02	80.4237	3.4517		6.41E-08	9.54E-06
21	20-21	3.93E-02	83.2226	3.5718		6.63E-08	9.60E-06
22	21-22	3.93E-02	86.0354	3.6925		6.86E-08	9.67E-06
23	22-23	3.94E-02	88.8624	3.8138		7.08E-08	9.74E-06
24	23-24	3.95E-02	91.7037	3.9358		7.31E-08	9.82E-06
25	24-25	3.96E-02	94.5596	4.0584		7.54E-08	9.89E-06
26	25-26	3.97E-02	97.4305	4.1816		7.77E-08	9.97E-06
27	26-27	3.97E-02	100.3165	4.3054		8.00E-08	1.00E-05
28	27-28	3.98E-02	103.2178	4.4299		8.23E-08	1.01E-05
29	28-29	3.99E-02	106.1347	4.5551		8.46E-08	1.02E-05
30	29-30	4.00E-02	109.0674	4.6810	9.45E-08	8.69E-08	1.03E-05
	Maximum Average Methane Concentration =			2.9373		1.64E-06	= Total Methane Flux Per Channel

PCE

Channel Element #	Depth (m)	mol fraction	Cg (g/m3)	C^g (g/m3)	Qj into Bottom of Channel Element (m^3/sec)	Mass Flux Across Wall (g/sec)	Mass Flux into Bottom of Channel Element (g/sec)	
0	Vadose Zone						4.88E-09	= Per Channel Flux of
1	0-1	1.97E-06	0.0157	0.0499		-2.37E-10	4.64E-09	PCE into Vadose Zone
2	1-2	1.87E-06	0.0163	0.0517		-2.16E-10	4.43E-09	
3	2-3	1.79E-06	0.0167	0.0532		-1.98E-10	4.23E-09	
4	3-4	1.71E-06	0.0172	0.0546		-1.81E-10	4.05E-09	
5	4-5	1.63E-06	0.0176	0.0558		-1.67E-10	3.88E-09	
6	5-6	1.56E-06	0.0179	0.0569		-1.54E-10	3.73E-09	
7	6-7	1.50E-06	0.0182	0.0579		-1.42E-10	3.58E-09	
8	7-8	1.44E-06	0.0185	0.0588		-1.31E-10	3.45E-09	
9	8-9	1.38E-06	0.0188	0.0597		-1.22E-10	3.33E-09	
10	9-10	1.33E-06	0.0190	0.0604		-1.13E-10	3.22E-09	
11	10-11	1.28E-06	0.0192	0.0611		-1.05E-10	3.11E-09	
12	11-12	1.24E-06	0.0194	0.0617		-9.83E-11	3.01E-09	
13	12-13	1.20E-06	0.0196	0.0622		-9.19E-11	2.92E-09	
14	13-14	1.16E-06	0.0197	0.0627		-8.61E-11	2.84E-09	
15	14-15	1.12E-06	0.0199	0.0631		-8.09E-11	2.76E-09	
16	15-16	1.08E-06	0.0200	0.0635		-7.63E-11	2.68E-09	
17	16-17	1.05E-06	0.0201	0.0639		-7.23E-11	2.61E-09	
18	17-18	1.02E-06	0.0202	0.0641		-6.91E-11	2.54E-09	
19	18-19	9.85E-07	0.0203	0.0643		-6.66E-11	2.47E-09	
20	19-20	9.54E-07	0.0203	0.0645		-6.54E-11	2.41E-09	
21	20-21	9.23E-07	0.0203	0.0644		-6.57E-11	2.34E-09	
22	21-22	8.92E-07	0.0202	0.0642		-6.83E-11	2.27E-09	
23	22-23	8.58E-07	0.0200	0.0637		-7.46E-11	2.20E-09	
24	23-24	8.19E-07	0.0197	0.0626		-8.68E-11	2.11E-09	
25	24-25	7.73E-07	0.0191	0.0608		-1.08E-10	2.00E-09	
26	25-26	7.13E-07	0.0181	0.0576		-1.46E-10	1.86E-09	
27	26-27	6.28E-07	0.0164	0.0522		-2.09E-10	1.65E-09	
28	27-28	5.04E-07	0.0135	0.0430		-3.18E-10	1.33E-09	
29	28-29	3.11E-07	0.0086	0.0272		-5.04E-10	8.25E-10	
30	29-30	0.00E+00	0.0000	0.0000	9.45E-08	-8.25E-10	0	

TCE

Channel Element #	Depth (m)	mol fraction	Cg (g/m3)	C^g (g/m3)	Qj Into Bottom of Channel Element (m3/sec)	Mass Flux Across Wall (g/sec)	Mass Flux Into Bottom of Channel Element (g/sec)	
0	Vadose Zone						3.07E-09	= Per Channel Flux of
1	0-1	1.55E-06	0.0098	0.0563		-1.79E-10	2.89E-09	TCE Into Vadose Zone
2	1-2	1.46E-06	0.0100	0.0577		-1.60E-10	2.73E-09	
3	2-3	1.38E-06	0.0103	0.0590		-1.44E-10	2.59E-09	
4	3-4	1.31E-06	0.0104	0.0600		-1.30E-10	2.46E-09	
5	4-5	1.24E-06	0.0106	0.0610		-1.18E-10	2.34E-09	
6	5-6	1.18E-06	0.0108	0.0618		-1.07E-10	2.24E-09	
7	6-7	1.13E-06	0.0109	0.0625		-9.75E-11	2.14E-09	
8	7-8	1.08E-06	0.0110	0.0632		-8.91E-11	2.05E-09	
9	8-9	1.03E-06	0.0111	0.0637		-8.17E-11	1.97E-09	
10	9-10	9.88E-07	0.0112	0.0642		-7.51E-11	1.89E-09	
11	10-11	9.49E-07	0.0113	0.0647		-6.92E-11	1.82E-09	
12	11-12	9.12E-07	0.0113	0.0651		-6.39E-11	1.76E-09	
13	12-13	8.78E-07	0.0114	0.0655		-5.91E-11	1.70E-09	
14	13-14	8.46E-07	0.0114	0.0658		-5.48E-11	1.65E-09	
15	14-15	8.17E-07	0.0115	0.0661		-5.09E-11	1.59E-09	
16	15-16	7.89E-07	0.0115	0.0664		-4.74E-11	1.55E-09	
17	16-17	7.63E-07	0.0116	0.0666		-4.42E-11	1.50E-09	
18	17-18	7.39E-07	0.0116	0.0668		-4.12E-11	1.46E-09	
19	18-19	7.16E-07	0.0117	0.0670		-3.86E-11	1.42E-09	
20	19-20	6.94E-07	0.0117	0.0672		-3.61E-11	1.39E-09	
21	20-21	6.74E-07	0.0117	0.0674		-3.39E-11	1.35E-09	
22	21-22	6.55E-07	0.0118	0.0676		-3.18E-11	1.32E-09	
23	22-23	6.36E-07	0.0118	0.0677		-2.99E-11	1.29E-09	
24	23-24	6.19E-07	0.0118	0.0678		-2.83E-11	1.26E-09	
25	24-25	6.02E-07	0.0118	0.0679		-2.71E-11	1.24E-09	
26	25-26	5.86E-07	0.0118	0.0679		-2.72E-11	1.21E-09	
27	26-27	5.67E-07	0.0117	0.0675		-3.27E-11	1.18E-09	
28	27-28	5.34E-07	0.0114	0.0653		-6.16E-11	1.11E-09	
29	28-29	4.34E-07	0.0095	0.0545		-2.02E-10	9.12E-10	
30	29-30	0.00	0.0000	0.0000	9.45E-08	-9.12E-10	0.00E+00	

INPUT DATA - HORIZONTAL SPARGE WELL

Groundwater Temperature ("T" °C)	Aquifer Porosity (decimal)	Seepage Velocity (m/day)	Min. Entry Pressure (m water)	Tortuosity Factor	l_t (mm)
10	0.25	2.7	0.20	0.6	1

Inject. Rate (ft^3/min)	Inject. Rate (m^3/sec)	Biozone Width (m)	Channel Interval (m)	Channel Radius (mm)	Well Length (m)
600	0.2834	60	1	2	2000

COMPOUND	m^1 (g/mol)	K_h @ T °C	D_w @ T °C (cm^3/sec)	x^1 in sparge gas (decimal)	C_o in groundwater (g/m^3)
Oxygen	32	25.6	1.50E-05	0.19	0.00
Nitrogen	28	52.3	1.21E-05	0.77	0.00
Methane	16	23.3	9.62E-06	0.04	0.00
PCE	165.8	0.31	6.10E-06	0.00	0.07
TCE	131.4	0.17	6.75E-06	0.00	0.07

CALCULATED CONSTANTS (at T °C)

Channels
120,000

Flow / Channel (m^3/sec)	$D'_{w\,eff}$ (cm^3/sec)
2.36E-06	2.25E-06
	1.82E-06
	1.44E-06
	9.15E-07
	1.01E-06

RESULTS

Total Oxygen Delivery (g/day)	Total Methane Delivery (g/day)
2.81E+04	2.09E+03

Average Oxygen Concentration (g/m3)	Average Methane Concentration (g/m3)
0.75	0.06

PCE Flux to Vadose Zone (g/sec-m^2)	TCE Flux to Vadose Zone (g/sec-m^2)
2.94E-09	3.20E-09

k' (m^3/g-day)	k bio (1/day)
0.1	0.004

EFFICIENCY: 0.09434

Oxygen

Channel Element #	Depth (m)	mol fraction	Cg (g/m3)	C^g (g/m3)	Qj into Bottom of Channel Element (m3/sec)	Mass Flux Across Wall (g/sec)	Mass Flux Into Bottom of Channel Element (g/sec)
0	Vadose Zone						2.44E-03
1	0-1	0.1899	292.30	11.42		3.98E-08	2.44E-03
2	1-2	0.1899	317.93	12.42		4.33E-08	2.44E-03
3	2-3	0.1899	343.57	13.42		4.68E-08	2.44E-03
4	3-4	0.1899	369.20	14.42		5.03E-08	2.44E-03
5	4-5	0.1899	394.84	15.42		5.38E-08	2.44E-03
6	5-6	0.1899	420.47	16.42		5.73E-08	2.44E-03
7	6-7	0.1899	446.11	17.43		6.08E-08	2.44E-03
8	7-8	0.1899	471.75	18.43		6.43E-08	2.44E-03
9	8-9	0.1899	497.39	19.43		6.77E-08'	2.44E-03
10	9-10	0.1899	523.03	20.43		7.12E-08	2.44E-03
11	10-11	0.1899	548.67	21.43		7.47E-08	2.44E-03
12	11-12	0.1899	574.32	22.43		7.82E-08	2.44E-03
13	12-13	0.1899	599.96	23.44		8.17E-08	2.44E-03
14	13-14	0.1899	625.60	24.44		8.52E-08	2.45E-03
15	14-15	0.1899	651.25	25.44		8.87E-08	2.45E-03
16	15-16	0.1899	676.90	26.44		9.22E-08	2.45E-03
17	16-17	0.1899	702.55	27.44		9.57E-08	2.45E-03
18	17-18	0.1899	728.20	28.45		9.92E-08	2.45E-03
19	18-19	0.1899	753.85	29.45		1.03E-07	2.45E-03
20	19-20	0.1900	779.50	30.45		1.06E-07	2.45E-03
21	20-21	0.1900	805.16	31.45		1.10E-07	2.45E-03
22	21-22	0.1900	830.82	32.45		1.13E-07	2.45E-03
23	22-23	0.1900	856.48	33.46		1.17E-07	2.45E-03
24	23-24	0.1900	882.14	34.46		1.20E-07	2.45E-03
25	24-25	0.1900	907.80	35.46		1.24E-07	2.45E-03
26	25-26	0.1900	933.46	36.46		1.27E-07	2.45E-03
27	26-27	0.1900	959.13	37.47		1.31E-07	2.45E-03
28	27-28	0.1900	984.80	38.47		1.34E-07	2.45E-03
29	28-29	0.1900	1010.47	39.47		1.38E-07	2.45E-03
30	29-30	0.1900	1036.14	40.47	2.36E-06	1.41E-07	2.45E-03
	Maximum Average Oxygen Concentration =			**25.94**		**2.71E-06**	**= Total Oxygen Flux Per Channel**

Nitrogen

Channel Element #	Depth (m)	mol fraction	Cg (g/m3)	C^g (g/m3)	Qj into Bottom of Channel Element (m3/sec)	Mass Flux Across Wall (g/sec)	Mass Flux Into Bottom of Channel Element (g/sec)
0	Vadose Zone						8.67E-03
1	0-1	0.7701	1037.19	19.83		5.58E-08	8.67E-03
2	1-2	0.7701	1128.14	21.57		6.07E-08	8.67E-03
3	2-3	0.7701	1219.08	23.31		6.56E-08	8.67E-03
4	3-4	0.7701	1310.03	25.05		7.05E-08	8.67E-03
5	4-5	0.7701	1400.97	26.79		7.54E-08	8.67E-03
6	5-6	0.7701	1491.92	28.53		8.03E-08	8.67E-03
7	6-7	0.7701	1582.86	30.27		8.52E-08	8.67E-03
8	7-8	0.7701	1673.80	32.00		9.01E-08	8.67E-03
9	8-9	0.7701	1764.74	33.74		9.50E-08	8.67E-03
10	9-10	0.7701	1855.68	35.48		9.99E-08	8.67E-03
11	10-11	0.7701	1946.62	37.22		1.05E-07	8.67E-03
12	11-12	0.7701	2037.56	38.96		1.10E-07	8.67E-03
13	12-13	0.7701	2128.50	40.70		1.15E-07	8.67E-03
14	13-14	0.7701	2219.43	42.44		1.19E-07	8.67E-03
15	14-15	0.7701	2310.37	44.18		1.24E-07	8.67E-03
16	15-16	0.7701	2401.30	45.91		1.29E-07	8.67E-03
17	16-17	0.7701	2492.23	47.65		1.34E-07	8.67E-03
18	17-18	0.7701	2583.16	49.39		1.39E-07	8.67E-03
19	18-19	0.7701	2674.09	51.13		1.44E-07	8.67E-03
20	19-20	0.7701	2765.02	52.87		1.49E-07	8.68E-03
21	20-21	0.7700	2855.95	54.61		1.54E-07	8.68E-03
22	21-22	0.7700	2946.87	56.35		1.59E-07	8.68E-03
23	22-23	0.7700	3037.80	58.08		1.64E-07	8.68E-03
24	23-24	0.7700	3128.72	59.82		1.68E-07	8.68E-03
25	24-25	0.7700	3219.64	61.56		1.73E-07	8.68E-03
26	25-26	0.7700	3310.55	63.30		1.78E-07	8.68E-03
27	26-27	0.7700	3401.47	65.04		1.83E-07	8.68E-03
28	27-28	0.7700	3492.38	66.78		1.88E-07	8.68E-03
29	28-29	0.7700	3583.30	68.51		1.93E-07	8.68E-03
30	29-30	0.7700	3674.21	70.25	2.36E-06	1.98E-07	8.68E-03

Methane

Channel Element #	Depth (m)	mol fraction	Cg (g/m3)	C^g (g/m3)	Qj into Bottom of Channel Element (m^3/sec)	Mass Flux Across Wall (g/sec)	Mass Flux Into Bottom of Channel Element (g/sec)
0	Vadose Zone						2.57E-04
1	0-1	4.00E-02	30.7782	1.3210		2.95E-09	2.57E-04
2	1-2	4.00E-02	33.4772	1.4368		3.21E-09	2.57E-04
3	2-3	4.00E-02	36.1762	1.5526		3.47E-09	2.57E-04
4	3-4	4.00E-02	38.8753	1.6685		3.73E-09	2.57E-04
5	4-5	4.00E-02	41.5743	1.7843		3.99E-09	2.57E-04
6	5-6	4.00E-02	44.2734	1.9001		4.25E-09	2.57E-04
7	6-7	4.00E-02	46.9726	2.0160		4.51E-09	2.57E-04
8	7-8	4.00E-02	49.6718	2.1318		4.76E-09	2.57E-04
9	8-9	4.00E-02	52.3710	2.2477		5.02E-09	2.57E-04
10	9-10	4.00E-02	55.0702	2.3635		5.28E-09	2.57E-04
11	10-11	4.00E-02	57.7695	2.4794		5.54E-09	2.57E-04
12	11-12	4.00E-02	60.4689	2.5952		5.80E-09	2.57E-04
13	12-13	4.00E-02	63.1683	2.7111		6.06E-09	2.57E-04
14	13-14	4.00E-02	65.8677	2.8269		6.32E-09	2.57E-04
15	14-15	4.00E-02	68.5672	2.9428		6.58E-09	2.57E-04
16	15-16	4.00E-02	71.2668	3.0587		6.84E-09	2.57E-04
17	16-17	4.00E-02	73.9664	3.1745		7.09E-09	2.57E-04
18	17-18	4.00E-02	76.6660	3.2904		7.35E-09	2.57E-04
19	18-19	4.00E-02	79.3658	3.4063		7.61E-09	2.57E-04
20	19-20	4.00E-02	82.0656	3.5221		7.87E-09	2.57E-04
21	20-21	4.00E-02	84.7654	3.6380		8.13E-09	2.57E-04
22	21-22	4.00E-02	87.4653	3.7539		8.39E-09	2.57E-04
23	22-23	4.00E-02	90.1653	3.8698		8.65E-09	2.58E-04
24	23-24	4.00E-02	92.8654	3.9856		8.91E-09	2.58E-04
25	24-25	4.00E-02	95.5655	4.1015		9.17E-09	2.58E-04
26	25-26	4.00E-02	98.2657	4.2174		9.43E-09	2.58E-04
27	26-27	4.00E-02	100.9660	4.3333		9.68E-09	2.58E-04
28	27-28	4.00E-02	103.6664	4.4492		9.94E-09	2.58E-04
29	28-29	4.00E-02	106.3668	4.5651		1.02E-08	2.58E-04
30	29-30	4.00E-02	109.0674	4.6810	2.36E-06	1.05E-08	2.58E-04
	Maximum Average Methane Concentration =			3.0008		2.01E-07	= Total Methane Flux Per Channel

PCE

Channel Element #	Depth (m)	mol fraction	Cg (g/m3)	C^g (g/m3)	Qj into Bottom of Channel Element (m^3/sec)	Mass Flux Across Wall (g/sec)	Mass Flux Into Bottom of Channel Element (g/sec)	
0	Vadose Zone						2.94E-09	= Per Channel Flux of
1	0-1	4.25E-08	0.0003	0.0011		-9.77E-11	2.84E-09	PCE Into Vadose Zone
2	1-2	4.11E-08	0.0004	0.0011		-9.76E-11	2.74E-09	
3	2-3	3.96E-08	0.0004	0.0012		-9.76E-11	2.64E-09	
4	3-4	3.82E-08	0.0004	0.0012		-9.75E-11	2.54E-09	
5	4-5	3.67E-08	0.0004	0.0013		-9.75E-11	2.45E-09	
6	5-6	3.52E-08	0.0004	0.0013		-9.74E-11	2.35E-09	
7	6-7	3.38E-08	0.0004	0.0013		-9.74E-11	2.25E-09	
8	7-8	3.23E-08	0.0004	0.0013		-9.74E-11	2.16E-09	
9	8-9	3.09E-08	0.0004	0.0013		-9.74E-11	2.06E-09	
10	9-10	2.94E-08	0.0004	0.0013		-9.73E-11	1.96E-09	
11	10-11	2.79E-08	0.0004	0.0013		-9.74E-11	1.86E-09	
12	11-12	2.65E-08	0.0004	0.0013		-9.74E-11	1.77E-09	
13	12-13	2.50E-08	0.0004	0.0013		-9.74E-11	1.67E-09	
14	13-14	2.36E-08	0.0004	0.0013		-9.74E-11	1.57E-09	
15	14-15	2.21E-08	0.0004	0.0012		-9.75E-11	1.47E-09	
16	15-16	2.06E-08	0.0004	0.0012		-9.75E-11	1.38E-09	
17	16-17	1.92E-08	0.0004	0.0012		-9.76E-11	1.28E-09	
18	17-18	1.77E-08	0.0004	0.0011		-9.77E-11	1.18E-09	
19	18-19	1.62E-08	0.0003	0.0011		-9.77E-11	1.08E-09	
20	19-20	1.48E-08	0.0003	0.0010		-9.78E-11	9.85E-10	
21	20-21	1.33E-08	0.0003	0.0009		-9.79E-11	8.87E-10	
22	21-22	1.18E-08	0.0003	0.0009		-9.80E-11	7.89E-10	
23	22-23	1.04E-08	0.0002	0.0008		-9.81E-11	6.91E-10	
24	23-24	8.89E-09	0.0002	0.0007		-9.83E-11	5.93E-10	
25	24-25	7.41E-09	0.0002	0.0006		-9.84E-11	4.94E-10	
26	25-26	5.93E-09	0.0002	0.0005		-9.86E-11	3.96E-10	
27	26-27	4.45E-09	0.0001	0.0004		-9.87E-11	2.97E-10	
28	27-28	2.97E-09	0.0001	0.0003		-9.89E-11	1.98E-10	
29	28-29	1.49E-09	0.0000	0.0001		-9.91E-11	9.92E-11	
30	29-30	0.00E+00	0.0000	0.0000	2.36E-06	-9.92E-11	0	

TCE

Channel Element #	Depth (m)	mol fraction	Cg (g/m3)	C^g (g/m3)	Qj into Bottom of Channel Element (m3/sec)	Mass Flux Across Wall (g/sec)	Mass Flux Into Bottom of Channel Element (g/sec)	
0	Vadose Zone						3.20E-09	= Per Channel Flux of
1	0-1	5.86E-08	0.0004	0.0021		-1.06E-10	3.10E-09	TCE into Vadose Zone
2	1-2	5.66E-08	0.0004	0.0022		-1.06E-10	2.99E-09	
3	2-3	5.46E-08	0.0004	0.0023		-1.06E-10	2.88E-09	
4	3-4	5.25E-08	0.0004	0.0024		-1.06E-10	2.78E-09	
5	4-5	5.05E-08	0.0004	0.0025		-1.06E-10	2.67E-09	
6	5-6	4.85E-08	0.0004	0.0025		-1.06E-10	2.57E-09	
7	6-7	4.65E-08	0.0004	0.0026		-1.06E-10	2.46E-09	
8	7-8	4.45E-08	0.0005	0.0026		-1.06E-10	2.35E-09	
9	8-9	4.25E-08	0.0005	0.0026		-1.06E-10	2.25E-09	
10	9-10	4.05E-08	0.0005	0.0026		-1.06E-10	2.14E-09	
11	10-11	3.85E-08	0.0005	0.0026		-1.06E-10	2.04E-09	
12	11-12	3.65E-08	0.0005	0.0026		-1.06E-10	1.93E-09	
13	12-13	3.45E-08	0.0004	0.0026		-1.06E-10	1.83E-09	
14	13-14	3.25E-08	0.0004	0.0025		-1.06E-10	1.72E-09	
15	14-15	3.05E-08	0.0004	0.0025		-1.06E-10	1.61E-09	
16	15-16	2.85E-08	0.0004	0.0024		-1.06E-10	1.51E-09	
17	16-17	2.65E-08	0.0004	0.0023		-1.06E-10	1.40E-09	
18	17-18	2.45E-08	0.0004	0.0022		-1.06E-10	1.30E-09	
19	18-19	2.25E-08	0.0004	0.0021		-1.06E-10	1.19E-09	
20	19-20	2.05E-08	0.0003	0.0020		-1.07E-10	1.08E-09	
21	20-21	1.84E-08	0.0003	0.0018		-1.07E-10	9.75E-10	
22	21-22	1.64E-08	0.0003	0.0017		-1.07E-10	8.68E-10	
23	22-23	1.44E-08	0.0003	0.0015		-1.07E-10	7.61E-10	
24	23-24	1.24E-08	0.0002	0.0014		-1.08E-10	6.53E-10	
25	24-25	1.03E-08	0.0002	0.0012		-1.08E-10	5.45E-10	
26	25-26	8.26E-09	0.0002	0.0010		-1.08E-10	4.37E-10	
27	26-27	6.21E-09	0.0001	0.0007		-1.09E-10	3.28E-10	
28	27-28	4.15E-09	0.0001	0.0005		-1.09E-10	2.19E-10	
29	28-29	2.08E-09	0.0000	0.0003		-1.09E-10	1.10E-10	
30	29-30	0.00	0.0000	0.0000	2.36E-06	-1.10E-10	0.00E+00	